Chem Soc Rev

REVIEW ARTICLE

View Article Online
View Journal | View Issue

Check for updates

Cite this: *Chem. Soc. Rev.*, 2021, **50**, 528

Received 2nd July 2020

DOI: 10.1039/d0cs00443j

rsc.li/chem-soc-rev

Published on 09 2020. Downloaded on 10/09/2024 14:36:19.

The rise of metal–organic polyhedra

Soochan Lee, Hyein Jeong, Dongsik Nam, Myoung Soo Lah * and Wonyoung Choe *

Metal–organic polyhedra are a member of metal–organic materials, and are together with metal–organic frameworks utilized as emerging porous platforms for numerous applications in energy- and bio-related sciences. However, metal–organic polyhedra have been significantly underexplored, unlike their metal–organic framework counterparts. In this review, we will cover the topologies and the classification of metal–organic polyhedra and share several suggestions, which might be useful to synthetic chemists regarding the future directions in this rapid-growing field.

1. Introduction

Polyhedra were discovered in the early stages of civilization in the east and the west and are found in art, science, architecture, and humanities to describe not only tangible objects but also metaphysical concepts, thus becoming a form of language. Some of the interesting examples are as follows. Polyhedron-shaped stones traced back to 2000 BC were found in Scotland.[1] Ancient people in Roman and Silla dynasties, although they were geometrically separated by the Eurasian continent, both played games with polyhedron-shaped dice.[2,3] Plato related five regular polyhedra to elements of the world: earth (cube), air (octahedron), fire (tetrahedron), water (icosahedron), and ether (dodecahedron) in the dialogue *Timaeus*.[4] Kepler modeled the solar system as nested polyhedra in his book *Mysterium Cosmographicum*, reflecting his theological ideas.[5] It is striking to note that a report in 2003 has suggested a dodecahedron as the shape of the universe.[6] Scientists have discovered polyhedra in nature at various length scales, from sub-nanometers and beyond, as exemplified by fullerenes,[7] the capsids of viruses,[8] quasi-crystals,[9] and metal nanoparticles.[10]

The rational design and synthesis of polyhedra using molecules and metals through coordination-driven self-assembly have been a fascinating research topic for synthetic chemists. Specifically, metal–organic polyhedra (MOPs),[11] assembled from organic linkers and metal-based secondary building units (SBUs),[12] are the examples of such endeavors, becoming an emerging class of metal–organic materials targeted for

Department of Chemistry, Ulsan National Institute of Science and Technology, UNIST-gil 50, Ulsan 44919, Republic of Korea. E-mail: mslah@unist.ac.kr, choe@unist.ac.kr

Soochan Lee

Soochan Lee received his BS degree from the Department of Chemistry at Ulsan National Institute of Science and Technology (UNIST) in 2017. He started a MS/PhD combined program in chemistry at UNIST. He is currently a PhD candidate in chemistry under the direction of Prof. Wonyoung Choe. His research focuses on the design and synthesis of new types of porous materials, including metal–organic polyhedra and zeolitic frameworks, for energy-related applications.

Hyein Jeong

Hyein Jeong received her BS from the Department of Chemistry at Ulsan National Institute of Science and Technology (UNIST) in 2018 and MS degree from the same department at the same school under the direction of Prof. Wonyoung Choe. Her research focuses on the design and synthesis of new types of metal–organic materials, such as metal–organic polyhedra and zeolitic-imidazolate frameworks, for finding novel properties of the materials.

This journal is © The Royal Society of Chemistry 2021

Published on 09 2020. Downloaded on 10/09/2024 14:36:19.

applications such as catalysis,[13,14] gas adsorption,[15,16] bio-related applications,[17,18] and membranes.[19–21] Yaghi and O'Keeffe devised a blueprint for MOPs, including geometric requirements for linkers and SBUs.[22] Thanks to in-depth knowledge of polyhedra and their self-assembly, accumulated over the past two decades, new MOPs are continuously reported in the literature, and will further flourish in existing and forthcoming applications.[23]

In this review, we focus on isolated MOPs instead of MOPs used as building blocks to build extended solids, *i.e.*, metal–organic frameworks (MOFs). For the readers interested in the latter topic, there are several excellent reviews available already.[24–26] Interestingly, MOPs have synthetic cousins, *e.g.*, cage compounds built from metal cations, and organic (mostly pyridyl-based) linkers. Fujita and others published reviews on these compounds.[27–29] For symmetry-guided synthesis approaches for MOPs and cage compounds, the reviews by Stang,[30,31] Yaghi,[22] and Raymond[32] provide essential information. The article by Alvarez is certainly a good read, with collections of polyhedra in chemistry, art, and history.[1] For readers interested in applications, there are several reviews on MOP applications up to 2016.[33–35]

This review has two goals: (i) to provide readers up-to-date information on types of MOPs, specifically, what they are and how they are classified, and (ii) to highlight new ideas/viewpoints for future directions in MOP assembly.

2. Classification of polyhedra

Polyhedra are three-dimensional objects with a finite number of vertices (corner points), edges (lines connecting pairs of vertices), and faces (polygonal surfaces). Polyhedra can be classified by their transitivity values (p,q,r), where p, q, and r are defined as the types of vertices, edges, and faces of the polyhedron, respectively (Table 1). The used three letter code for polyhedron topology as '**xyz**' is from the three-letter code of the Reticular Chemistry Structure Resource (RCSR) database (Fig. 1).[36] Popular polyhedra are regular, quasi-regular, and semi-regular ones.

Regular (Platonic) polyhedra are vertex-transitive (one kind of vertex), edge-transitive (one kind of edge), and face-transitive (one kind of face). The tetrahedron (**tet**), cube (**cub**), octahedron (**oct**), dodecahedron (**dod**), and icosahedron (**ico**) are five different regular polyhedra with transitivity values of (1,1,1).

Quasi-regular polyhedra are vertex- and edge-transitive but not face transitive. The cuboctahedron (**cuo**) and icosidodecahedron (**ido**) are two different quasi-regular polyhedra with transitivity values of (1,1,2). The duals[37] of quasi-regular polyhedra are face- and edge-transitive but not vertex-transitive. The dual of a **cuo** is a rhombic dodecahedron (**rdo**) of transitivity (2,1,1).

Semi-regular polyhedra are vertex-transitive but not edge-transitive polyhedra with regular polygonal faces. Truncated regular polyhedra (**tte**, **tcu**, **tro**, **tdo**, and **tic**) and prisms and antiprisms (**trp**, **sap**, **hpr**, **hap**) are semi-regular polyhedra.

Dongsik Nam

Dongsik Nam received his BS degree in chemistry (2016) from the Ulsan National Institute of Science and Technology (UNIST). He started a combined M.S./PhD program in chemistry at UNIST. He is currently a PhD candidate under the supervision of Prof. Wonyoung Choe. His research focuses on the design of new porous solids by self-assembly of metal–organic polyhedra.

Myoung Soo Lah

Myoung Soo Lah attended Seoul National University, Korea, for his BSc and MSc and earned his PhD in chemistry from the University of Michigan, Ann Arbor, in 1991. After his postdoctoral research in macromolecular crystallography from the same university, he became a faculty member of the department of chemistry, Hanyang University in 1992 and then moved to Ulsan National Institute of Science and Technology in 2010, where he is presently a professor of the department of chemistry. He is interested in the development of metal–organic systems such as MOPs and MOFs for application in the areas of storage, capture/separation, and catalysis.

Wonyoung Choe

Wonyoung Choe received his BS, MS, and PhD from Seoul National University, Seoul National University, and University of Michigan, Ann Arbor, respectively. After finishing his postdoctoral work at Iowa State University and Lawrence Livermore National Laboratory, USA, he became an assistant professor at University of Nebraska-Lincoln. In 2012, he moved to Korea and joined Ulsan National Institute of Science and Technology as a faculty member. Throughout his career, his main research interests have been solids, ranging from intermetallics to soft materials such as metal–organic frameworks and metal–organic polyhedra, for both fundamental and sustainable science.

Table 1 Basic structural information for the eighteen polyhedra

Polyhedron	Type of vertex, p	Type of edge, q	Type of face, r	Number of vertices	Number of edges	Number of faces	Dual polyhedron	Symmetry
tet	1	1	1	4	6	4	**tet**	T_d
oct	1	1	1	6	12	8	**cub**	O_h
cub	1	1	1	8	12	6	**oct**	O_h
dod	1	1	1	20	30	12	**ico**	I_h
ico	1	1	1	12	30	20	**dod**	I_h
cuo	1	1	2	12	24	14	**rdo**	O_h
ido	1	1	2	30	60	32	**trc**	I_h
rdo	2	1	1	14	24	12	**cuo**	O_h
trc	2	1	1	32	60	30	**ido**	I_h
trp	1	2	2	6	9	5	**tbp**	D_{3h}
twc	2	4	3	12	24	14	—	D_{3h}
mtq-d	2	2	3	9	18	11	**mtq**	D_{3h}
bds	2	4	2	8	18	12	**bds-d**	D_{2d}
ghm	4	4	4	20	36	18	—	D_{2d}
tct	2	3	3	9	21	14	**tct-d**	D_{3h}
hmg	5	5	3	23	42	21	—	D_{3h}
csa	2	3	2	10	24	16	**csa-d**	D_{4d}
xum	4	5	4	26	48	24	—	D_{4d}

Published on 09 2020. Downloaded on 10/09/2024 14:36:19.

Semi-regular convex polyhedra excluding prisms and antiprisms are called Archimedean solids, and the duals of Archimedean solids are called Catalan solids.

When polyhedral species are assembled using inorganic and organic building blocks, becoming MOPs, the vertices of the MOPs are either polytopic inorganic or organic nodes (branch points in the organic building block), and the edges of the MOPs are the linkers between the inorganic nodes and/or between inorganic and organic nodes. To form finite polyhedral species, at least one of the building blocks must be bent or curved.

3. SBUs and linkers for MOP construction

Careful choice of organic linkers and metal SBUs is the key to build the desired MOP topology. We would like to show the representative SBUs and organic linkers in Fig. 2–5. For convenience, k-coordinated nodes (nodes with k links) are referred to as k-c nodes.[38] In this review, we will cover 3-c, 4-c, and 5-c metal-based SBUs (Fig. 2), 2-c organic linkers (linear and bent) (Fig. 3 and 4, respectively), and unusual organic linkers as 3-c nodes (Fig. 5) for MOP assembly. The combination of these structure building blocks shows 14 polyhedra, as shown in Table 2.

4. Regular polyhedra

4.1. Tetrahedron (tet)

The tetrahedron is the simplest of all the convex polyhedra, composed of four vertices, six edges, and four triangular faces. In the assembly of metal–organic tetrahedra, four SBUs as 3-c nodes are linked by six organic 2-c linkers, forming tetrahedron topology, denoted by **tet**, the RCSR three-letter code. In this section, we survey **tet**-MOPs assembled from different types of SBUs.

$[Fe_3O(SO_4)_3(py)_3]_4A_6$. The M_3O SBU, forming a trigonal prism with six carboxylates, has been frequently used in various MOFs.[39–41] For example, in MIL-101, a supertetrahedron with 4 M_3O SBUs and organic ligands generate remarkable nanosized hierarchical pores.[41] Yaghi *et al.* reported an isoreticular series of MOPs assembled from 3-connected Fe_3O clusters and ditopic organic linkers by blocking binding sites with SO_4^{2-} counter anions.[15] The resulting 3-c Fe_3O cluster $[Fe_3O(SO_4)_3(py_3)]$ (py = pyridine) was capped with three bridging sulfate groups located on one side of the trigonal prism and three pyridines to offer octahedral coordination to the Fe atoms. These clusters connect with three carboxylates arranged at 60° angles and thus serve as 3-c SBUs. The resulting MOPs were assembled from four $[Fe_3O(SO_4)_3(py_3)]$ clusters and six ditopic linkers (**A1** for IRMOP-50, **A5** for IRMOP-51, **A6** for IRMOP-52, and **A8** for IRMOP-53). The sizes of the **tet**-MOPs and pores increased with increasing ligand size, but the tetrahedron geometry remained unchanged (Fig. 6). Such isoreticular expansion is common in MOFs[42] and can be extended to MOPs. Notably, IRMOP-51 and -53 showed permanent porosity and various gas adsorption capabilities. For example, the hydrogen uptake of IRMOP-51 was comparable with that of MOF-5, exhibiting 81% of its v/v hydrogen capability.

$[Cp_2Zr_3O(OH)_3]_4A_6$. A notable series of emerging MOPs have been the Zr-based MOPs with high chemical and mechanical stability. Although MOFs with Zr clusters have been extensively studied, because of their structural robustness, originated from the high affinities between the oxophilic Zr cations and carboxylate groups,[43] Zr-based MOPs started to appear in some recent reports.[13,44–50] The first report of Zr-based MOPs by Yuan *et al.* presented tetrahedral MOPs, composed of trinuclear Zr clusters $[Cp_3Zr_3O(OH)_3$, Cp = η^5-$C_5H_5]$.[44] Considering a plane connecting three Zr cations, the carboxylate linkers are below the plane while the Cp rings are above the plane, providing an ideal SBU geometry as the vertices of tetrahedra. In addition to the tetrahedral cages, ligand variations resulted in several types of Zr-based MOPs, including heterocubes, and cubes with identical Zr clusters.

 This journal is © The Royal Society of Chemistry 2021

Published on 09 2020. Downloaded on 10/09/2024 14:36:19.

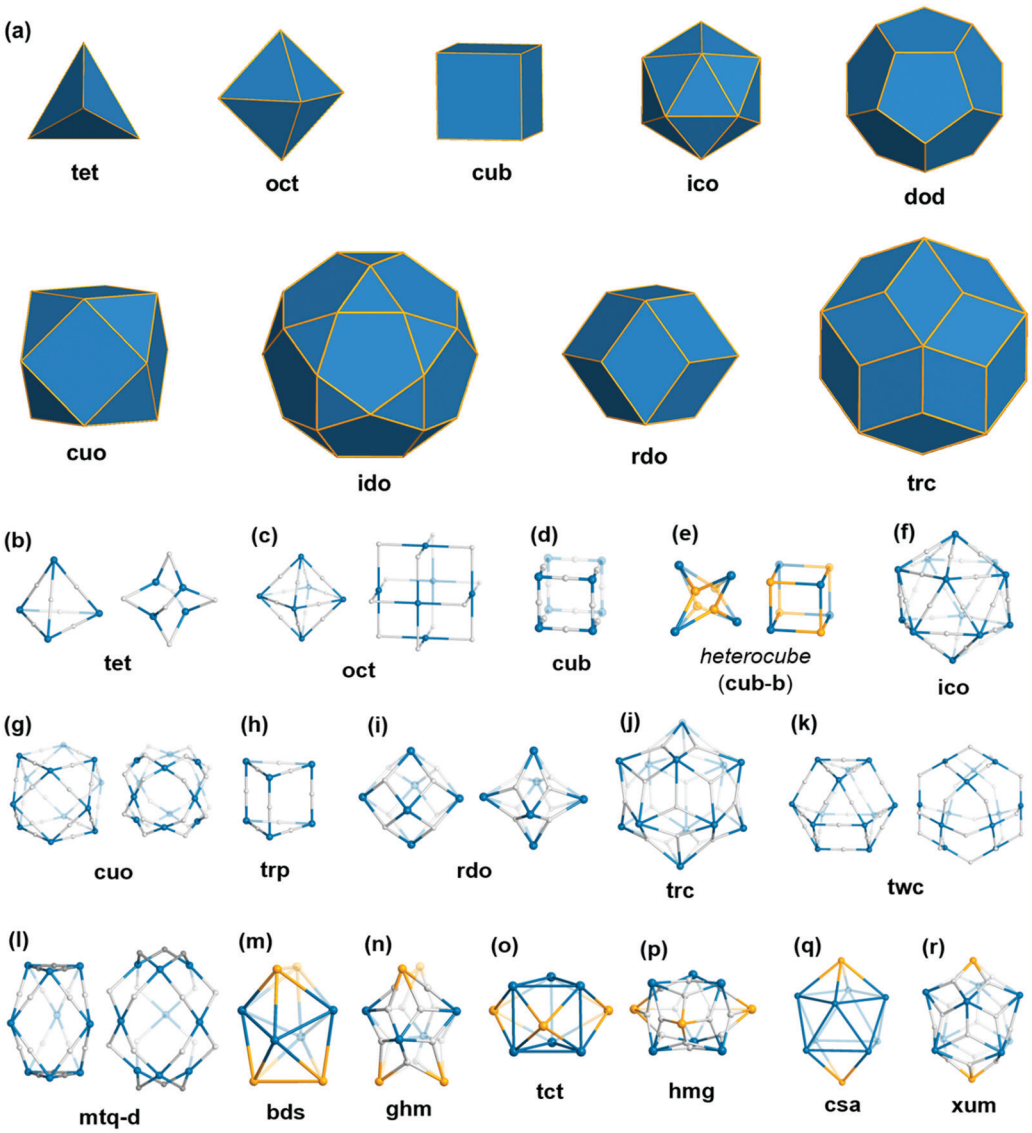

Fig. 1 Description of the polyhedra covered in this review. The three boldfaced letters (**xyz**) are the RCSR code for the polyhedra.[22] (a) Nine edge-transitive polyhedra, specifically the five regular solids, *i.e.*, tetrahedron (**tet**), octahedron (**oct**), cube (**cub**), icosahedron (**ico**), dodecahedron (**dod**), two quasi-regular solids, *i.e.*, cuboctahedron (**cuo**), icosidodecahedron (**ido**), and Catalan solids as duals of the quasi-regular solids, *i.e.*, rhombic dodecahedron (**rdo**) and rhombic triacontahedron (**trc**). (b)–(r) The skeletal view of 17 polyhedra covered in this review, including the heterocube (**cub-b**), triangular prism (**trp**), anticuboctahedron (**twc**), hendecahedron (**mtq-d**), snub disphenoid and face-capped snub disphenoid (**bds**, **ghm**), triaugmented triangular prism and face-capped triaugmented triangular prism (**tct**, **hmg**), and gyroelongated square bipyramid and face-capped gyroelongated square bipyramid (**csa**, **xum**).

Tetrahedral cages can be formed with four zirconium clusters and six linear ditopic linkers ($[Cp_2Zr_3O(OH)_3]_4\mathbf{A}_6$). Representative examples are the ZrT series (Fig. 7).[44] Using the **A1** linker, a tetrahedral MOP (ZrT-1, $[Cp_3Zr_3O(OH)_3]_4(\mathbf{A1})_6$) was prepared. A larger tetrahedral cage (ZrT-3, $[Cp_3Zr_3O(OH)_3]_4(\mathbf{A5})_6$) was synthesized using the **A5** linker. Both MOPs showed permanent porosity, as confirmed by N_2 adsorption. Regarding chemical stability, mass spectra revealed the intact cages in acetonitrile/water solutions under various pH conditions (2.2–9.8).[48]

When functionalized linkers are utilized, interesting chemical variations of tetrahedral cages are also possible. One such example is MOPs with **A9** linkers, which can coordinate with metal cations such as Cu^{2+} and Pd^{2+}.[45] For example, Zr-bpydc ($[Cp_3Zr_3O(OH)_3]_4(\mathbf{A9})_6$) with pyridyl groups on the edges of a tetrahedral cage was successfully synthesized. By adding copper and palladium salts in a solution of reactants, Zr-bpydc-$CuCl_2$ ($[Cp_3Zr_3O(OH)_3]_4(\mathbf{A10})_6$) and Zr-bpydc-$PdCl_2$ ($[Cp_3Zr_3O(OH)_3]_4(\mathbf{A11})_6$) were prepared *via* post-synthetic metal installation.

Another example is the tetrahedral cages with chiral organic linkers.[13] The linkers are **A12**, **A13**, and **A14**, which are salen-based chiral metalloligands. MOPs, $[Cp_3Zr_3O(OH)_3]_4$ (**A12** or **A13**)$_6$, were prepared with enantiopure **A12** and **A13** (Fig. 8). Three more MOPs were synthesized by mixing two types of

Published on 09 2020. Downloaded on 10/09/2024 14:36:19.

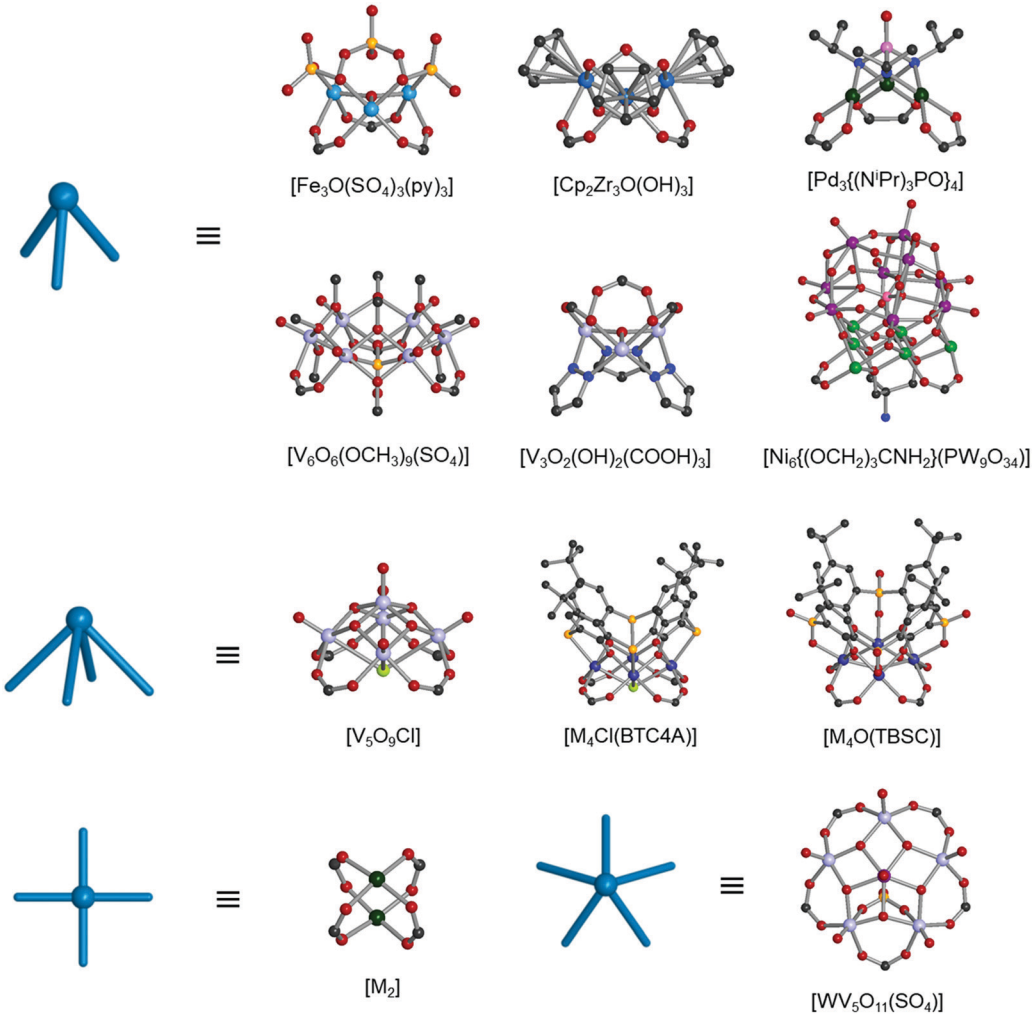

Fig. 2 The list of metal cluster-based SBUs. The first and second rows show the 3-c nodes with 60° coordination angles, $[Fe_3O(SO_4)_3(py)_3]$, $[Cp_2Zr_3O(OH)_3]$, $[Pd_3\{(N^iPr)_3PO\}_4]$, $[V_6O_6(OCH_3)_9(SO_4)]$, $[V_3O_2(OH)_2(COOH)_3]$, and $[Ni_6\{(OCH_2)_3CNH_2\}(PW_9O_{34})]$. The third row shows the 4-c nodes with 60° coordination angles, $[V_5O_9Cl]$, $[M_4Cl(BTC4A)]$, and $[M_4O(TBSC)]$. The fourth row shows the 4-c node with a square-planar coordination geometry, $[M_2]$, and the 5-c node with a 60° coordination angle, $[WV_5O_{11}(SO_4)]$.

linkers (Mn/Cr, Mn/Fe, and Cr/Fe) in a 1 : 1 molar ratio. MOPs with single **A12** and **A13** were analyzed with single-crystal X-ray diffraction (SCXRD). The structures were distorted tetrahedral cages without a linker disorder. In the two MOP structures, all the linkers retained their chirality. A total of five MOPs, including three mixed-linker MOPs, exhibited similar powder X-ray diffraction (PXRD) patterns and homochirality from the circular dichroism spectra. These mixed-linker MOPs were investigated for sequential asymmetric catalysis, resulting in enhanced properties in epoxidation and ring-opening reactions.

The Choe group reported a **tet**-Zr-MOP, UMOP-1-NH_2, $[Cp_3Zr_3O(OH)_3]_4(\mathbf{A2})_6$, employing 2-aminoterephthalic acid ($\mathbf{H_2A2}$).[46] Compared to **ZrT-1**, UMOP-1-NH_2 showed similar tetrahedral cages with disordered amine groups in four sites of each phenyl ring. The cages were stable in water and methanol. UMOP-1-NH_2 was further investigated as a building block for organic condensation reactions, leading to cross-linked tetrahedral cages with flexible alkyl chains. The amine-functionalized cage was also utilized in post-synthetic linker modification, confirmed by mass spectrometry.[48]

$[V_3O_2(OH)_2(COOH)_3]_4A_6$ and $[V_6O_6(OCH_3)_9(XO_4)]_4A_6$, X = S or V. Polyoxometalates (POMs), high-valent early transition metal-oxide anions with structural and functional diversity, are attractive inorganic molecules because of their potential applications in catalysis, magnetism, medicine, and the field of nano/electrochemistry.[51–53] POMs have been popular as SBUs for inorganic–organic hybrid materials due to their high connectivity and large-sized clusters.[54,55] Among the POMs, polyoxovanadates (POVs) produced various types of coordination molecular cages when combined with organic linkers.

Navarro *et al.* reported a **tet**-MOP, constructed from trinuclear POV and ditopic pyrazolate ligands, instead of carboxylate ligands.[56] Four $[V_3O_2(OH)_2(COOH)_3]$ clusters were connected by pyrazolate with six **A18** linkers (Fig. 9). This MOP exhibited permanent porosity, selective adsorption of CO_2 over N_2, and volatile organic compound separation properties for benzene/cyclohexane.

 This journal is © The Royal Society of Chemistry 2021

Published on 09 2020. Downloaded on 10/09/2024 14:36:19.

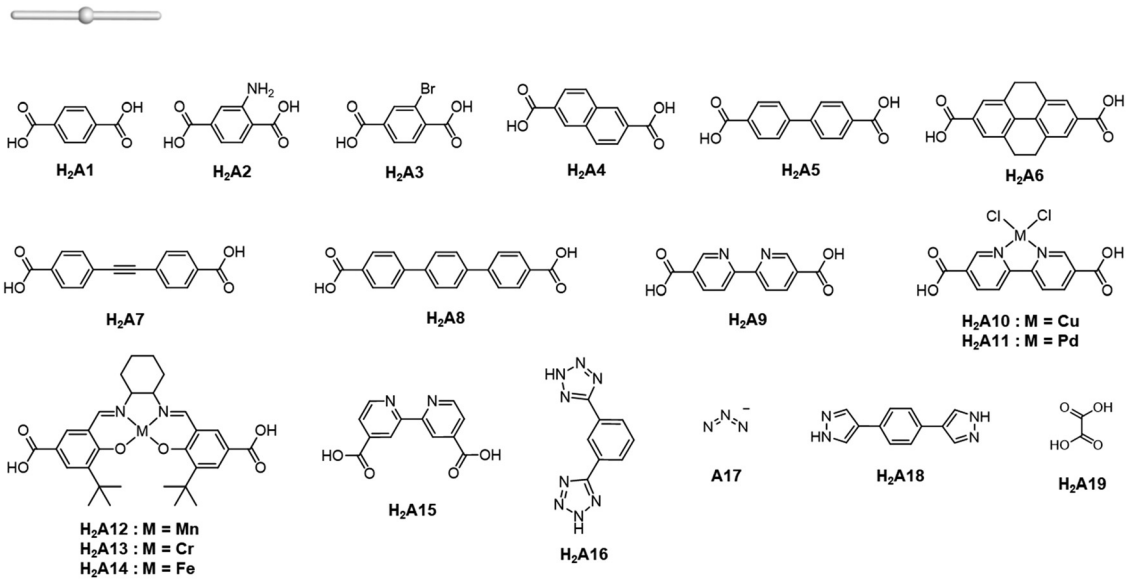

Fig. 3 Linear ditopic organic ligands as linear linkers to construct MOPs. **H_2A1**: 1,4-benzenedicarboxylic acid; **H_2A2**: 2-amino-1,4-benzenedicarboxylic acid; **H_2A3**: 2-bromo-1,4-benzenedicarboxylic acid; **H_2A4**: 2,6-naphthalenedicarboxylic acid; **H_2A5**: 1,1′-biphenyl-4,4′-dicarboxylic acid; **H_2A6**: 4,5,9,10-tetrahydropyrene-2,7-dicarboxylic acid; **H_2A7**: 4,4′-(ethyne-1,2-diyl)dibenzoic acid; **H_2A8**: 1,1′:4′,1″-terphenyl-4,4″-dicarboxylic acid; **H_2A9**: 2,2′-bipyridine-5,5′-dicarboxylic acid; **H_2A10**: copper dichloride 2,2′-bipyridine-5,5′-dicarboxylic acid; **H_2A11**: palladium dichloride 2,2′-bipyridine-5,5′-dicarboxylic acid; **H_2A12**: *N,N*′-bis(3-*tert*-butyl-5-(carboxyl))salicylidene-1,2-cyclohexanediamine-manganese; **H_2A13**: *N,N*′-bis(3-*tert*-butyl-5-(carboxyl))salicylidene-1,2-cyclohexanediamine-chromium; **H_2A14**: *N,N*′-bis(3-*tert*-butyl-5-(carboxyl))salicylidene-1,2-cyclohexanediamine-iron; **H_2A15**: 2,2′-bipyridine-4,4′-dicarboxylic acid; **H_2A16**: 1,3-di(1*H*-tetrazol-5-yl)benzene; **A17**: azide; **H_2A18**: 1,4-di(1*H*-pyrazol-4-yl)benzene; and **H_2A19**: oxalic acid.

The Su group has successfully demonstrated the reticular synthesis of POV-based MOPs. They showed an unprecedented alkoxo-POV as an SBU for MOPs. The alkoxo-POV, $[V_6O_6(OCH_3)_9(\mu_6\text{-}SO_4)]$, composed of a hexavanadium sulfur core $\{V_6S\}$, nine methoxy bridging groups, and six oxo anions, offered 3-c coordinate environments for tetrahedron formation.[57] The modular tetrahedral MOPs were assembled from four alkoxo-POV and six ditopic linear ligands for VMOP-11, -12, and -13 (**A1** for VMOP-11, **A2** for VMOP-12 and **A3** for VMOP-13) (Fig. 9). Instead of a $\{V_6S\}$ cluster, an unprecedented $\{V_7\}$ alkoxo-POV was also obtained from a different metal source (VCl_3 for $\{V_7\}$ and $VOSO_4{\cdot}xH_2O$ for $\{V_6S\}$).[58] The reactions with four $[V_6O_6(OCH_3)_9(VO_4)]$ clusters and ditopic **A1** and **A2** ligands afforded VMOP-16 and -17 with tetrahedral geometry. These were isostructures to VMOP-11 and -12. A recent report by Su and coworkers showed a larger VMOP composed of $[V_6O_6(OCH_3)_9(\mu_6\text{-}SO_4)]$ clusters and 4,4′-(ethyne-1,2-diyl)dibenzoate (**A7**) linkers.[59]

$[Pd_3\{(N^iPr)_3PO\}_4]_4A_6$. The d^8 metal ions are suitable components for building coordination compounds due to their highly predictable coordination environment.[27,28,31] In particular, palladium(II) ions strongly prefer a square-planar coordination geometry, widely utilized to construct polyhedron-shaped coordination cages.[27,28] Despite the coordination polyhedra, successfully synthesized with a single Pd(II) center, multi-nuclear Pd clusters are rather scarce in MOP chemistry. Boomishankar *et al.* reported a **tet**-MOP assembly with novel Pd_3 clusters that were capped by tris(alkylimido)phosphate trianions, $[(N^iPr)_3PO]^{3-}$ (^iPr = iso-propyl). The cluster formula was $Pd_3[(N^iPr)_3PO]$.[60] Synthesis with 3-c Pd_3 clusters and linear ditopic carboxylates afforded tetrahedral cage assemblies in MOP synthesis. The neutral tetrahedron-shaped $[(Pd_3[(N^iPr)_3PO])_4(\mathbf{A19})_6]$ was assembled by the bridging of six ditopic oxalate linkers between Pd_3 clusters, serving as a 3-c SBU for edge-transitive tetrahedron geometry (Fig. 10). The porosity of this cage was verified by a CO_2-sorption experiment at 195 K, and the encapsulation of polar and nonpolar solvent molecules was observed from host–guest studies in solution and the solid-state.

$[(Mo_2)(t\text{-}Bu\text{-}CO_2)]_4B_6$. In a rare case, the 3-c node in **tet**-MOPs has different coordination bond angles instead of the typical 60° bond angle. Pamore *et al.* synthesized a Mo_2 paddlewheel SBU-based tetrahedron.[61] Mo_2 units capped by *tert*-butyl carboxylate (t-Bu-CO_2) were connected by three **B1** linkers in a T-shaped bridging environment (two at 90° and one at 180°; average: 120°). The formula of the assembled tetrahedron was $[(Mo_2)_4(t\text{-}Bu\text{-}CO_2)_4(\mathbf{B1})_6]$. Due to the T-shaped SBU connection, the carboxylates in the **B1** linker were twisted and located out of the thiophene plane. Such distorted molecular geometry is shown in Fig. 11.

4.2. Octahedron (oct)

An octahedron is a regular convex polyhedron, composed of six vertices, twelve edges, and eight triangular faces. The dual polyhedron of an octahedron is a cube. To construct a molecularly self-assembled octahedron, six 4-c SBUs at the vertices and twelve bridging linkers are required. The RCSR code for an octahedron is **oct**. The ideal assembly of an **oct** MOP is the linkage of tetravalent SBUs with 60° coordination bond angles

Published on 09 2020. Downloaded on 10/09/2024 14:36:19.

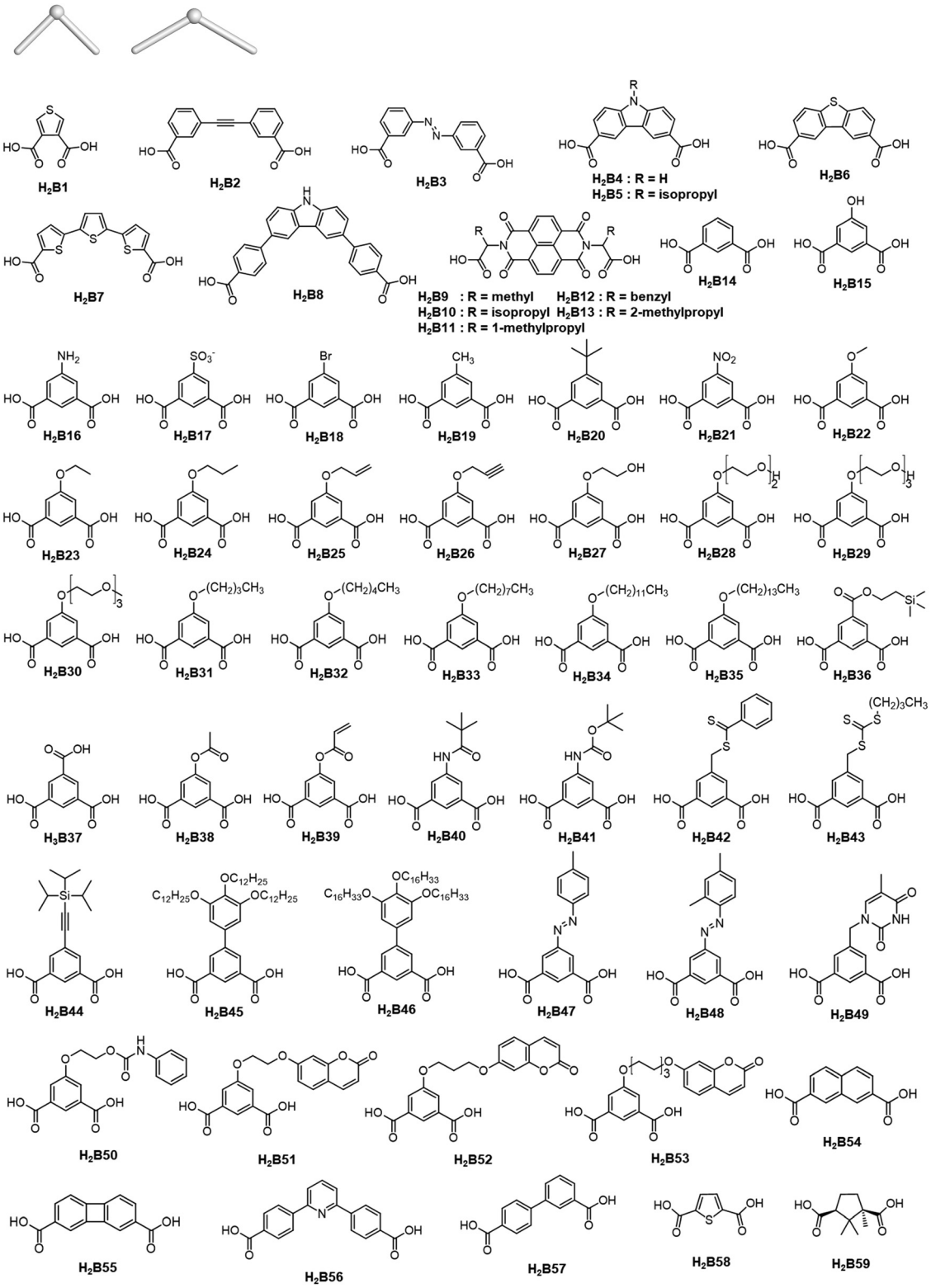

Fig. 4 Bent ditopic organic ligands as bent linkers to construct MOPs. **H_2B1**: thiophene-3,4-dicarboxylic acid; **H_2B2**: 3,3′-(1,2-ethynediyl)dibenzoic acid; **H_2B3**: azobenzene-3,3′-dicarboxylic acid; **H_2B4**: 9*H*-carbazole-3,6-dicarboxylic acid; **H_2B5**: 9-isopropyl-9*H*-carbazole-3,6-dicarboxylic acid; **H_2B6**: 2,8-dibenzothiophenedicarboxylic acid; **H_2B7**: 2,2′:5′,2″-terthiophene-5,5″-dicarboxylic acid; **H_2B8**: 4,4′-(9*H*-carbazole-3,6-diyl)dibenzoic acid; **H_2B9**: 2,2′-(1,3,6,8-tetraoxo-1,3,6,8-tetrahydrobenzo[*lmn*][3,8]phenanthroline-2,7-diyl)dipropionic acid; **H_2B10**: 2,2′-(1,3,6,8-tetraoxo-1,3,6,8-tetrahydrobenzo[*lmn*][3,8]phenanthroline-2,7-diyl)bis(3-methylbutanoic acid); **H_2B11**: 2,2′-(1,3,6,8-tetraoxo-1,3,6,8-tetrahydrobenzo[*lmn*][3,8]phenanthroline-2,7-diyl)bis(3-methylpentanoic acid); **H_2B12**: 2,2′-(1,3,6,8-tetraoxo-1,3,6,8-tetrahydrobenzo[*lmn*][3,8]phenanthroline-2,7-diyl)bis(3-phenylpropanoic acid); **H_2B13**: 2,2′-(1,3,6,8-tetraoxo-1,3,6,8-tetrahydrobenzo[*lmn*][3,8]phenanthroline-2,7-diyl)bis(4-methylpentanoic acid); **H_2B14**: 1,3-benzenedicarboxylic acid; **H_2B15**: 5-hydroxy-1,3-benzenedicarboxylic acid; **H_2B16**: 5-amino-1,3-benzenedicarboxylic acid; **H_2B17**: 5-sulfo-1,3-benzenedicarboxylic acid;

 This journal is © The Royal Society of Chemistry 2021

H_2B18: 5-bromo-1,3-benzenedicarboxylic acid; **H_2B19**: 5-methyl-1,3-benzenedicarboxylic acid; **H_2B20**: 5-*tert*-butyl-1,3-benzenedicarboxylic acid; **H_2B21**: 5-nitro-1,3-benzenedicarboxylic acid; **H_2B22**: 5-methoxy-1,3-benzenedicarboxylic acid; **H_2B23**: 5-ethoxy-1,3-benzenedicarboxylic acid; **H_2B24**: 5-*n*-propyloxy-1,3-benzenedicarboxylic acid; **H_2B25**: 5-allyloxo-1,3-benzenedicarboxylic acid; **H_2B26**: 5-prop-2-ynyloxy-1,3-benzenedicarboxylic acid; **H_2B27**: 5-(2-hydroxyethoxy)-1,3-benzenedicarboxylic acid; **H_2B28**: 5-(2-(2-hydroxyethoxy)ethoxy)-1,3-benzenedicarboxylic acid; **H_2B29**: 5-(2-(2-(2-hydroxyethoxy)ethoxy)ethoxy)-1,3-benzenedicarboxylic acid; **H_2B30**: 5-(2-(2-(2-methoxyethoxy)ethoxy)ethoxy)-1,3-benzenedicarboxylic acid; **H_2B31**: 5-*n*-butyloxy-1,3-benzenedicarboxylic acid; **H_2B32**: 5-*n*-pentyloxy-1,3-benzenedicarboxylic acid; **H_2B33**: 5-*n*-octyloxy-1,3-benzenedicarboxylic acid; **H_2B34**: 5-*n*-dodecyloxy-1,3-benzenedicarboxylic acid; **H_2B35**: 5-*n*-tetradecyloxy-1,3-benzenedicarboxylic acid; **H_2B36**: 5-((2-(trimethylsilyl)ethoxy)carbonyl)isophthalic acid; **H_3B37**: 1,3,5-benzenetricarboxylic acid; **H_2B38**: 5-(acetyloxy)isophthalic acid; **H_2B39**: 5-(acryloyloxy)isophthalic acid; **H_2B40**: 5-*tert*-butylamide-1,3-benzenedicarboxylic acid; **H_2B41**: 5-((*tert*-butoxycarbonyl)amino)isophthalic acid; **H_2B42**: 5-[[(phenylthioxomethyl)thio]methyl]-1,3-benzenedicarboxylic acid; **H_2B43**: 5-[[[(butylthio)thioxomethyl]thio]methyl]-1,3-benzenedicarboxylic acid; **H_2B44**: 5-(triisopropylsilyl)ethynyl-1,3-benzenedicarboxylic acid; **H_2B45**: 3′,4′,5′-tris(dodecyloxy)-[1,1′-biphenyl]-3,5-dicarboxylic acid; **H_2B46**: 3′,4′,5′-tris(hexadecyloxy)-[1,1′-biphenyl]-3,5-dicarboxylic acid; **H_2B47**: 5-(*p*-tolyldiazenyl)-1,3-benzenedicarboxylic acid; **H_2B48**: 5-(2,4-dimethylphenyldiazenyl)-1,3-benzenedicarboxylic acid; **H_2B49**: 5-(5-methyl-2,4-dioxo-3,4-dihydropyrimidin-1(2*H*)-yl)methyl-1,3-benzenedicarboxylic acid; **H_2B50**: 5-{2-[(phenylcarbamoyl)oxy]ethoxy}-1,3-benzenedicarboxylic acid; **H_2B51**: 5-[2-[(2-oxo-2*H*-1-benzopyran-7-yl)oxy]ethoxy]-1,3-benzenedicarboxylic acid; **H_2B52**: 5-[3-[(2-oxo-2*H*-1-benzopyran-7-yl)oxy]propoxy]-1,3-benzenedicarboxylic acid; **H_2B53**: 5-[[6-[(2-oxo-2*H*-1-benzopyran-7-yl)oxy]hexyl]oxy]-1,3-benzenedicarboxylic acid; **H_2B54**: 2,7-naphthalenedicarboxylic acid; **H_2B55**: 2,7-biphenylenedicarboxylic acid; **H_2B56**: 4,4′-(pyridine-2,6-diyl)dibenzoic acid; **H_2B57**: biphenyl-3,4′-dicarboxylic acid; **H_2B58**: thiophene-2,5-dicarboxylic acid; and **H_2B59**: (1*R*,3*S*)-1,2,2-trimethylcyclopentane-1,3-dicarboxylic acid.

Published on 09 2020. Downloaded on 10/09/2024 14:36:19.

needed for the ditopic linkers. A previous review noted the lack of tetravalent metal SBUs with 60° coordination bond angles for **oct** MOPs.[22] In this section, we cover various types of octahedron-shaped MOPs constructed from various SBUs with 60° or 90° coordination.

$[V_5O_9Cl]_6A_{12}$. Due to various oxidation states and numbers of vanadium cations on POV clusters, the connectivity of POV SBUs can be modulated by the synthesis method. The **tet**-MOPs are commonly formed using 3-c POVs, while **oct**-MOPs are expected from 4-c POVs.

Nanosized octahedron-shaped MOPs were synthesized from an assembly with six 4-c polyoxo $[V_5O_9Cl]$ clusters and twelve ditopic carboxylate ligands by Su *et al.* (**A1** for VMOP-1, **A2** for VMOP-2, and **A3** for VMOP-3) (Fig. 12).[62] Their molecular sizes are roughly 2.5 nm. As can be seen in VMOP-6, the isoreticular pore expansion is possible by using an extended organic linker, **A4**.[63] The 4-c $[V_5O_9Cl]$ SBU is good for building octahedral architectures.

$[M_4Cl(BTC4A)]_6A_{12}$ and $[M_4O(TBSC)]_6A_{12}$. Calixarenes are macrocyclic molecules with basket shapes and have been extensively utilized as cavitands in host–guest chemistry due to their versatile conformations.[64] In supramolecular chemistry, calixarenes are popular choices for making capsule-like assembled supermolecules directed by simultaneous coordination and covalent bonds.[65–67] In particular, the cone formation of calix[4]arene's four hydroxyl groups at the lower rim offers potential as 4-c SBUs.

Hong *et al.* reported an **oct**-MOP constructed from *p-tert*-butylthiacalix[4]arene (H_4BTC4A), **A1** linkers, and Co(II) cations.[68] The post-assembly of deprotonated BTC4A anions and four Co(II) metal cations produced the tetranuclear and 4-c SBU, with the formula $[Co_4(BTC4A)(\mu_4\text{-}Cl)]$. Six $[Co_4(BTC4A)Cl]$ nodes were linked by twelve ditopic **A1** linkers with 60° coordination bond angles at the SBU center (Fig. 13). The formula for the **oct**-MOP was $[(Co_4(BTC4A)(\mu_4\text{-}Cl))_6(\mathbf{A1})_{12}]$. This MOP exhibited permanent porosity, possibly due to its rigid molecular construction.

Similarly, Wang's group introduced **oct**-MOPs based on different calix[4]arenes.[69] Instead of BTC4A, the calixarenes used were *p-tert*-butylsulfonylcalix[4]arene (H_4TBSC), *p-tert*-pentylsulfonylcalix[4]arene (H_4TPSC), and *p-tert*-octylsulfonylcalix[4]arene (H_4TOSC) for the assembly of **oct**-MOPs. In the case of TBSC, Co(II) or Ni(II) cations and **A1** linkers afforded the octahedral MOSC-II-*t*Bu-M (M = Co or Ni) (Fig. 13). The coordination environment was slightly different with Hong's **oct**-MOP. The divalent metal cations formed coordination bonds, retaining the octahedral coordination geometry with one oxygen from the sulfonyl group, one oxygen from the hydroxyl group, two oxygens of carboxylate coordination, and one of μ_4-H_2O molecule, with the **oct**-MOP formula of $[M_4(TBSC)(\mu_4\text{-}H_2O)]_6(\mathbf{A1})_{12}$, M = Co or Ni. Interestingly, the extrinsic pores were controlled by the length of the aliphatic moieties of sulfonylcalix[4]arenes. The molecular size of the **oct**-MOP series increased in the following order: MOSC-II-*t*Bu-M, MOSC-II-tPen-M, and MOSC-II-tOc-M. However, the inner pore sizes of the MOPs were practically the same. Only MOSC-II-tPen-Ni showed selective adsorption of O_2 (3.46 Å; kinetic diameter) over N_2 (3.64 Å) from the different guest inclusion sizes of the extrinsic pores, due to the modulated aliphatic moieties after removal of solvent molecules.

Chiral metallosalen complexes are well-known asymmetric catalysts for reactions such as the epoxidation of olefins and oxidative kinetic resolution (OKR) of racemic alcohols. Cui *et al.* designed and synthesized a chiral metallosalen-based **oct**-MOP.[14] The features of the assembly were similar to the MOSC-II-*t*Bu series. The six 4-c $[Zn_4O(TBSC)]$ SBUs were connected with twelve linear enantiopure (*R*,*R*)-**A12** groups. The assembled metallosalen-based **oct**-MOP contained $[Zn_4O(TBSC)]_6(\mathbf{A12})_{12}$, with a size of approximately 4.5 nm (Fig. 13). The efficient and enhanced enantioselectivity was verified for the OKR of secondary alcohols by supramolecular asymmetric catalysis from a metallosalen-based **oct**-MOP.

The octahedral coordination cages by mixing two $[M_4Cl(BTC4A)]$ and four $[M_4(SO_4)(BTC4A)]$ (M = Co or Fe) were synthesized with eight **A15** linkers.[70] Unlike the above-mentioned calixarene-based **oct**-MOPs, the anion, especially SO_4^{2-}, played a critical role in cage formation. Two **A15** linker moieties connected four $[M_4(SO_4)(BTC4A)]$ SBUs in the equatorial position. One direction of coordination was pyridyl

Published on 09 2020. Downloaded on 10/09/2024 14:36:19.

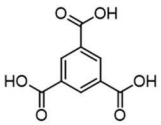

$H_3C1 = H_3B37$

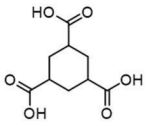

H_3C2

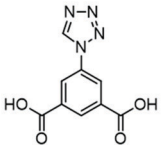

H_2C3

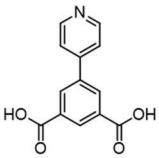

H_2C4

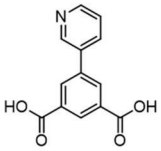

H_2C5

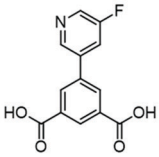

H_2C6

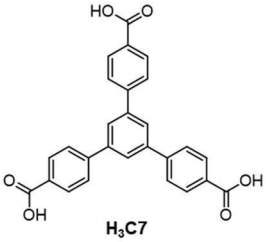

H_3C7

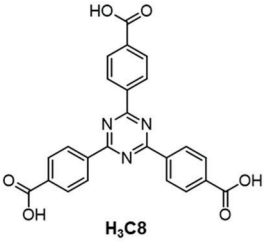

H_3C8

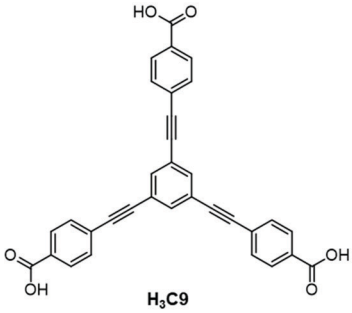

H_3C9

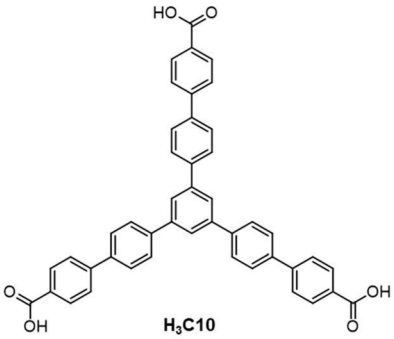

H_3C10

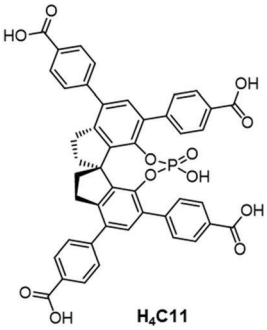

H_4C11

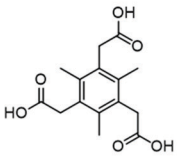

H_3C12

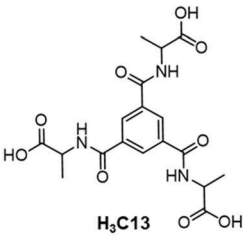

H_3C13

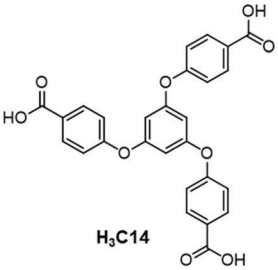

H_3C14

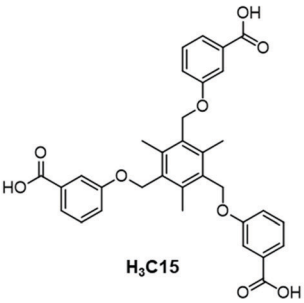

H_3C15

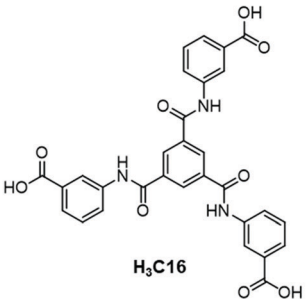

H_3C16

Fig. 5 Tritopic organic ligands as planar 3-c nodes (used as faces) to construct MOPs. **H_3C1**: 1,3,5-benzenetricarboxylic acid; **H_3C2**: cyclohexane-1,3,5-tricarboxylic acid; **H_2C3**: 5-(1*H*-tetrazol-5-yl)isophthalic acid; **H_2C4**: 5-(pyridin-4-yl)isophthalic acid; **H_2C5**: 5-(pyridine-3-yl)isophthalic acid; **H_2C6**: 5-(5-fluoropyridin-3-yl)isophthalic acid; **H_3C7**: 1,3,5-tris(4-carboxyphenyl)benzene; **H_3C8**: 4,4′,4″-(1,3,5-triazine-2,4,6-triyl)tribenzoic acid; **H_3C9**: 4,4′,4″-(benzene-1,3,5-triyltris(ethyne-2,1-diyl))tribenzoic acid; **H_3C10**: 4,4′,4″-(benzene-1,3,5-triyl-tris(benzene-4,1-diyl))tribenzoic acid; **H_4C11**: 4,4′,6,6′-tetrakis(4-benzoic acid)-1,1′-spinolphosphonate; **H_3C12**: 2,2′,2″-(2,4,6-trimethylbenzene-1,3,5-triyl)triacetic acid; **H_3C13**: 2,2′,2″-((benzene-1,3,5-tricarbonyl)tris(azanediyl))tripropionic acid; **H_3C14**: 4,4′,4″-(benzene-1,3,5-triyltris(oxy))tribenzoic acid; **H_3C15**: 3,3′,3″-(((2,4,6-trimethylbenzene-1,3,5-triyl)tris(methylene))tris(oxy))tribenzoic acid; **H_3C16**: 3,3′,3″-[1,3,5-benzenetriyltris(carbonylimino)]tris-benzoic acid.

 This journal is © The Royal Society of Chemistry 2021

Published on 09 2020. Downloaded on 10/09/2024 14:36:19.

Table 2 Polyhedral topologies assembled from combinations of nodes and linkers

	SBU node			
Organic linker	3-c node	4-c node	5-c node	4-c and 5-c nodes
2-c linker	tet, cub, trp	oct, cuo, twc, mtq-d	ico	—
3-c linker (node)	Heterocube (cub-b)	rdo	trc	ghm, hmg, xum

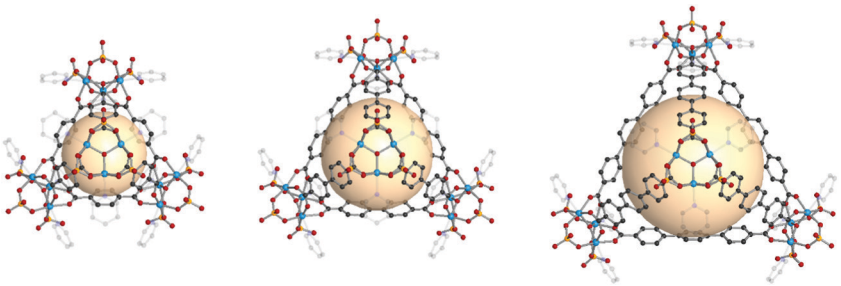

Fig. 6 Structural illustration of IRMOP-50, $[Fe_3O(SO_4)_3(py_3)]_4$(**A1**)$_6$ (left), IRMOP-51, $[Fe_3O(SO_4)_3(py_3)]_4$(**A5**)$_6$ (middle), and IRMOP-53, $[Fe_3O(SO_4)_3(py_3)]_4$(**A8**)$_6$ (right).[15]

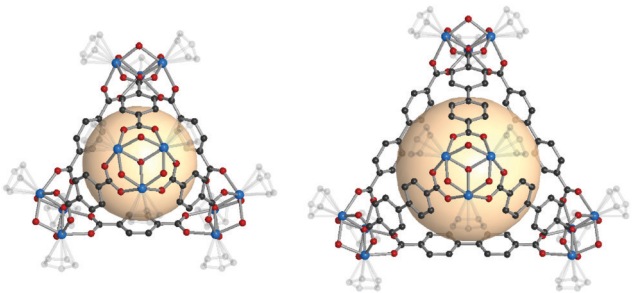

Fig. 7 Structural illustration of ZrT-1, $[Cp_3Zr_3O(OH)_3]_4$(**A1**)$_6$ (left) and ZrT-3, $[Cp_3Zr_3O(OH)_3]_4$(**A5**)$_6$ (right).[44]

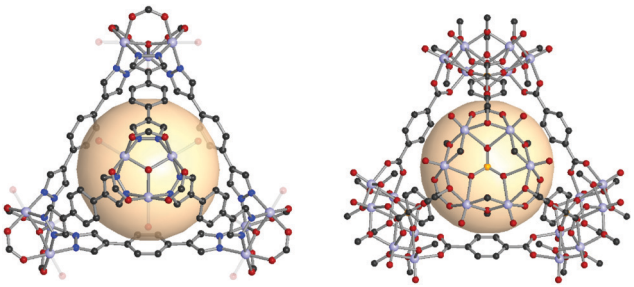

Fig. 9 Structural illustration of $[V_3O_2(OH)_2(COOH)_3]_4$(**A18**)$_6$ (left)[56] and **VMOP-11**, $[V_6O_6(OCH_3)_9(SO_4)]_4$(**A1**)$_6$ (right).[57]

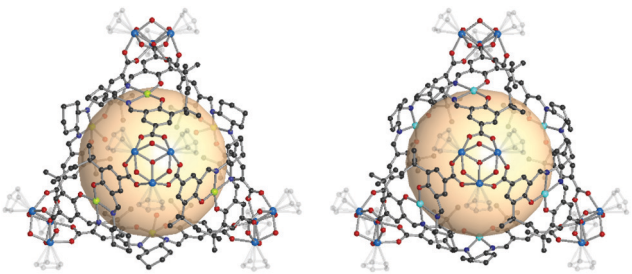

Fig. 8 Structural illustration of $[Cp_3Zr_3O(OH)_3]_4$(**A12**)$_6$ (left) and $[Cp_3Zr_3O(OH)_3]_4$(**A13**)$_6$ (right).[13]

binding, and another was carboxylate coordination to $[M_4(SO_4)(BTC4A)]$. Two $[M_4Cl(BTC4A)]$ in the axial position were bridged with one of the carboxylates in the **A15** linker in the same manner as other oct-MOPs. The fascinating [6+8] condensation afforded the abnormal octahedral cages of $[M_4Cl(BTC4A)]_2[M_4(SO_4)(BTC4A)]_4$(**A15**)$_8$.

$(M_2)_6B_{12}$. Dimetal paddlewheel M_2 (mostly Cu_2) components are one of the most frequently used SBUs to construct metal–organic materials, including MOFs and MOPs.[71] Square planar 4-c nodes offer a wide variety of structures, depending on the ligand geometry of the bridging carboxylates. To assemble **oct**-MOPs with M_2 paddlewheels, ditopic organic linkers with

Published on 09 2020. Downloaded on 10/09/2024 14:36:19.

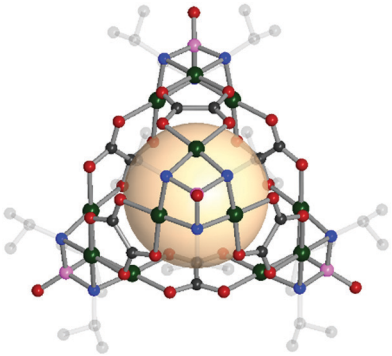

Fig. 10 Structural illustration of $[(Pd_3[(N^iPr)_3PO])_4(\mathbf{A19})_6]$.[60]

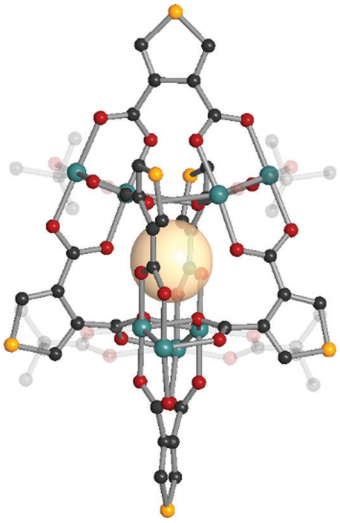

Fig. 11 Structural illustration of $[(Mo_2)_4(t\text{-Bu-CO}_2)_4(\mathbf{B1})_6]$.[61]

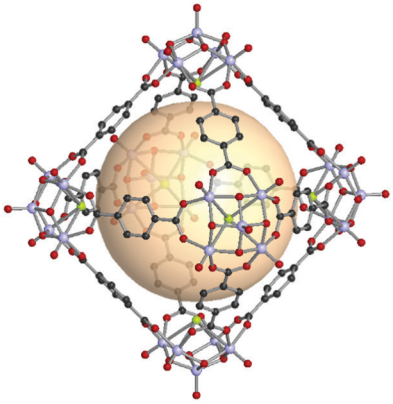

Fig. 12 Structural illustration of **VMOP-1**, $[V_5O_9Cl]_6(\mathbf{A1})_{12}$.[62]

90° bent angles are needed. The organic linkers used for M_2 based **oct**-MOPs are shown in Fig. 14.

The first type of linker is 9-R-3,6-carbazoledicarboxylate (R = H or ^{i}Pr). Zhou *et al.* synthesized an **oct**-MOP using six Cu_2 and twelve 9*H*-3,6-carbazoledicarboxylate (**B4**) building blocks (Fig. 14).[72] The synthesis procedure was different from the typical one-pot solvothermal synthesis. A solution of the pre-synthesized Cu_2-based lantern-type cage and excess **B4** linkers afforded the single-crystal **oct**-MOP, $(Cu_2)_6(\mathbf{B4})_{12}$. The Zhou group introduced a solvothermal synthesis of quadruply-bonded Mo_2-based **oct**-MOPs using **B4** linkers.[73] The Mo-Mo dimer, $Mo_2(CF_3CO_2)_4$, was used as a metal source to construct the rigid Mo_2 **oct**-MOP, $(Mo_2)_6(\mathbf{B4})_{12}$. Dinuclear Ru_2 has shown catalytic activity due to its redox-active core, which makes the building block desired for catalytic applications. Zhou *et al.* also reported Ru_2-based **oct**-MOPs with **B4** linkers, $(Ru_2)_6(\mathbf{B4})_{12}$.[74] The synthesis from two different oxidation states of Ru sources, $Ru_2(OAc)_4Cl$ and $Ru_2(OAc)_4$ (OAc = acetate), produced the same **oct**-MOP. The Bloch group recently synthesized a similar counterpart, $(Cr_2)_6(\mathbf{B4})_{12}$,[75] highly stable in desolvated conditions, unlike other M_2-based MOPs. Due to its remarkable stability, $(Cr_2)_6(\mathbf{B4})_{12}$ showed the highest Brunauer–Emmett–Teller surface area of all the octahedral M_2 MOPs. They also successfully synthesized Ni_2- and Co_2-based **oct**-MOPs using 9-isopropyl-3,6-carbazoledicaroxylate (**B5**).[76] In the synthesis of Ni_2 and Co_2 **oct**-MOPs, only **B5** afforded polyhedron structures ($(M_2)_6(\mathbf{B5})_{12}$, M = Ni or Co), and **B4** produced a two-dimensional MOF. This result clearly demonstrated the importance of ligand functionality to control the dimensionality of the phases. In addition to carbazole-based linkers, the dibenzothiophene linker (**B6**) with similar bent angles was utilized for the synthesis of the Cu_2 **oct**-MOP by Duan and coworkers.[77]

The second type of linker is 2,2′:5′,2″-terthiophene-5,5″-dicarboxylate (**B7**). The bent angle of **B7** was 90° with the *cis, cis* conformation. The Yaghi group synthesized an octahedral Cu_2-based MOP with **B7** linkers, MOP-28 (Fig. 14).[78] The formula was $(Cu_2)_6(\mathbf{B7})_{12}$. The pore size of MOP-28 was slightly larger than that of the $(M_2)_6(\mathbf{B4})_{12}$ octahedral MOP. The permanent and high porosity of MOP-28 was verified.

The third type of linker is the extended molecular structure of **B4**, 4,4′-(9*H*-carbazole-3,6-diyl)dibenzoate (**B8**). Zhou *et al.* synthesized a series of Mo_2-based **oct** MOPs using **B4**, **B8**, and **B4** with a phenyl ring added (Fig. 14).[73] The molecular size of the $(Mo_2)_6(\mathbf{B8})_{12}$ MOP was roughly 3.5 nm. Due to phenyl ring rotation by steric hindrance, the cage was slightly distorted compared to **B4**-based MOPs.

Another linker type for octahedral MOPs includes naphthalene diimide-based linkers.[79,80] Mollick *et al.* utilized linkers with a naphthalene diimide core and terminal amino acid moieties (**B9** to **B12**), leading to bent angles of carboxylic acid groups.[79] Four Cu_2-based octahedral MOPs were prepared with different amino acid moieties, alanine, valine, isoleucine, and phenylalanine, and increased chemical stability was shown. Boer *et al.* prepared a similar octahedral cage with a leucine-substituted naphthalene diimide linker (**B13**) and demonstrated enantioselective sorption and release of small analytes.[80]

Thus far, we have introduced examples of nearly regular octahedral M_2-based MOPs that were comprised of one type of linker with 90° bent angles. Surprisingly, synthesis using two mixed linkers, one with a 60° bent angle and the other with a 120° bent angle (average 90°), can afford distorted octahedral MOPs. A post-reaction using a solution of pre-synthesized

 This journal is © The Royal Society of Chemistry 2021

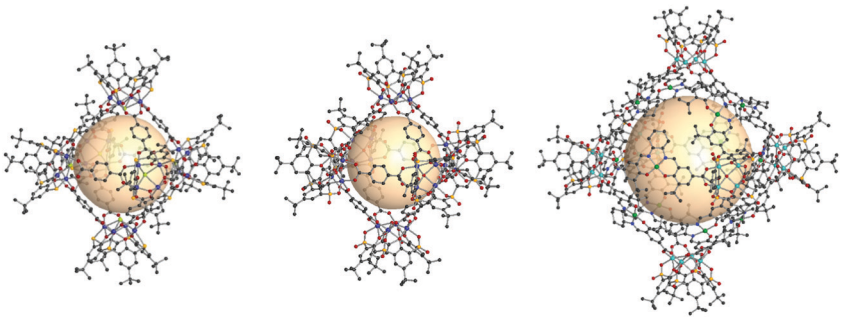

Fig. 13 Structural illustration of $[Co_4Cl(BTC4A)]_6(\mathbf{A1})_{12}$ (left),[68] $[Co_4O(TBSC)]_6(\mathbf{A1})_{12}$ (middle),[69] and $[Zn_4O(TBSC)]_6(\mathbf{A12})_{12}$ (right).[14]

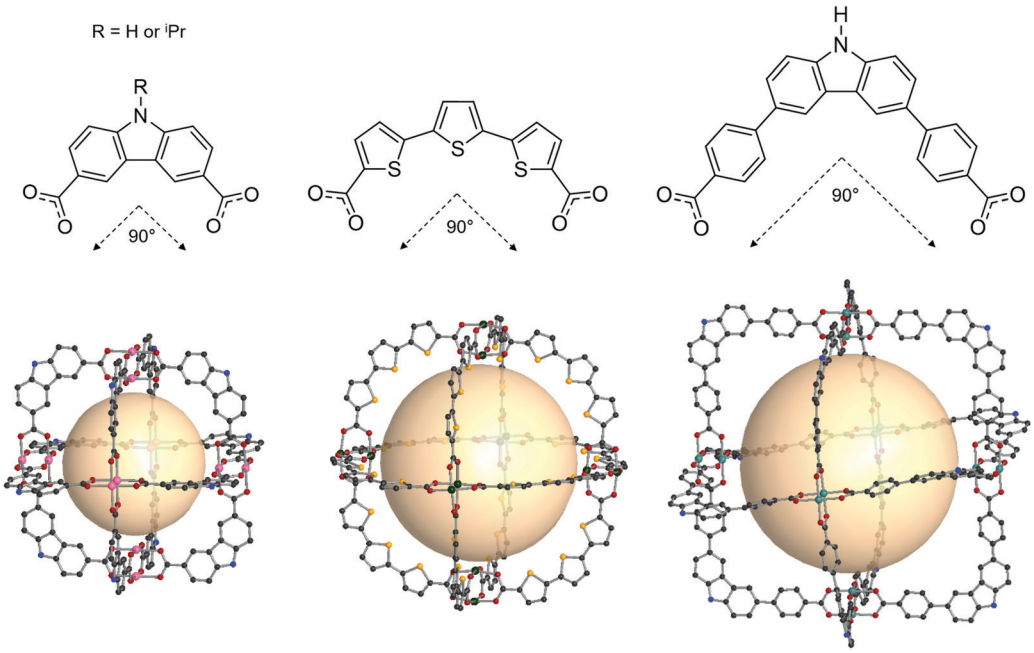

Fig. 14 Chemical diagram of **B4** and **B5**, **B7**, and **B8** ligands, which have 90° bent angles, and an architectural illustration of the **oct** MOPs resulting from the combination of M_2 nodes and each linker.[72,73,78]

Published on 09 2020. Downloaded on 10/09/2024 14:36:19.

cuboctahedron-shaped Cu_2 MOPs, composed of **B20** and excess of 3,3′-(ethyne-1,2-diyl)-dibenzoate (**B2**), was used to synthesize the distorted octahedral MOP, $(Cu_2)_6(\mathbf{B20})_6(\mathbf{B2})_6$ (Fig. 15).[72] The positions of the six **B2** linkers were equatorial, and six **B20** were located at the top and bottom connected by three linkers in the MOP. Similarly, Kitagawa *et al.* reported the distorted **oct**-MOP, $(Cu_2)_6(\mathbf{B20})_6(\mathbf{B3})_6$, using azobenzene-3,3′-dicarboxylate (**B3**) instead of **B2**.[81] This anisotropic linker position was utilized to introduce a polymeric moiety to the **B20** position.

4.3. Cube (cub)

A cube, also known as a regular hexahedron, has eight vertices, twelve edges, and six square faces. The dual polyhedron of a cube is an octahedron. Eight 3-c SBUs and twelve linkers on the edges are needed to construct a cube-type assembly, denoted as **cub** in the RCSR code. The cube is a polyhedron example to perfectly fill the three-dimensional space itself and is a highly promising molecular building block to form diverse architectures. Nevertheless, known examples of **cub**-MOPs are still rare, compared to **tet**- and **oct**-MOPs. The formation of **cub**-MOPs typically competes with the **tet**-MOP formation, when ditopic linkers are employed. We cover three types of **cub**-MOPs, constructed from various SBUs and organic linkers.

$\mathbf{[Ni_6\{(OCH_2)_3CNH_2\}(PW_9O_{34})]_8B_{12}}$. Yang *et al.* reported a rare example of the polyoxometalate-organic hybrid polyhedron.[82] The polyoxometalate $[Ni_6(Tris)(en)_3(B\text{-}\alpha\text{-}PW_9O_{34})]$ (Tris = $((OCH_2)_3CNH_2)^{3-}$, and en = $C_2H_4(NH_2)_2$) SBU, denoted as Ni_6PW_9, was constructed by capping Keggin B-α-PW_9O_{34} units on Tris-grafted Ni_6 cores. Two carboxylate units of twelve **B37** were coordinated to a Ni core in eight Ni_6PW_9 as an SBU. The assembled POM-based MOP was a cubic cage (Fig. 16). This is the only example of a cube-shaped and POM-based MOP.

$\mathbf{[Cp_2Zr_3O(OH)_3]_8B_{12}}$. A cubic Zr-MOP (HCCF-1, $[Cp_3Zr_3O(OH)_3]_8(\mathbf{B59})_{12}$) was formed with Zr clusters at the eight vertices and dicarboxylate linkers at the twelve edges (Fig. 17).[47] **B59** includes a five-membered carbon ring and methyl groups,

Published on 09 2020. Downloaded on 10/09/2024 14:36:19.

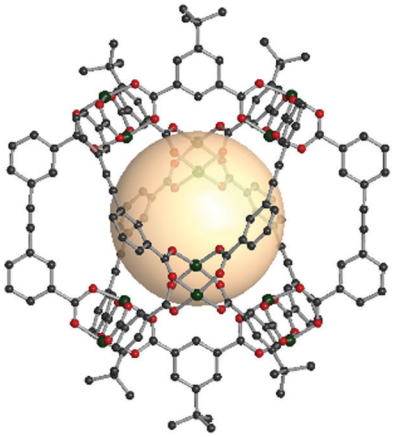

Fig. 15 Structural illustration of the distorted **oct** MOP, $(Cu_2)_6$(**B20**)$_6$(**B2**)$_6$.[72]

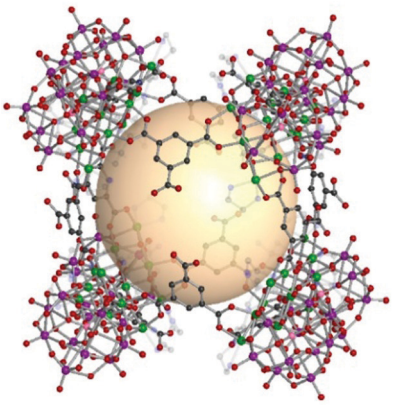

Fig. 16 Structural illustration of $[Ni_6\{(OCH_2)_3CNH_2\}(PW_9O_{34})]_8$(**B37**)$_{12}$.[82]

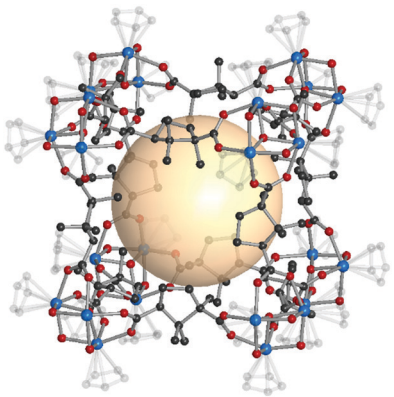

Fig. 17 Structural illustration of HCCF-1, $[Cp_3Zr_3O(OH)_3]_8$(**B59**)$_{12}$.[47]

leading to a bent shape. The reported HCCF-1 crystal structure showed disordered positions of the linkers. Due to the high number of hydrogen bonds between the cubic cages (O–H···Cl···H–O), HCCF-1 retained crystallinity after desolvation and exhibited microporosity.

$[M_4Cl(BTC4A)]_8A_{12}$. Liao *et al.* reported a unique type of **cub**-MOP, CIAC-108, based on the calix[4]arene SBU,

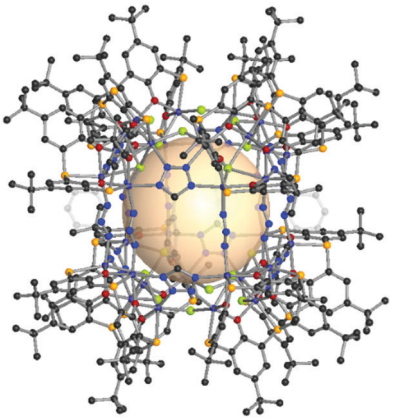

Fig. 18 Structural illustration of CIAC-108, $[\{Co_4(BTC4A)(\mu_4\text{-}Cl)\}_8$(**A16**)$_4$-(**A17**)$_8(\mu_2\text{-}Cl)_8]$.[83]

$[Co_4(BTC4A)(\mu_4\text{-}Cl)]$ cluster, used to build **oct**-MOPs (Fig. 18).[83] There are two different ditopic linkers, **A16** and **A17**. Interestingly, the former **A16** linker was prepared by an *in situ* click reaction with 1,3-dicyanobenzene and NaN_3 during one-pot synthesis. The two tetrazole moieties in **A16** connect the SBUs by occupying eight of the top and bottom edges. The remaining 4 edges in the equatorial positions in the cube were linked by eight N_3^- linkers, and each edge was occupied by two azide linkers. The formula of CIAC-108 was $[\{Co_4(BTC4A)(\mu_4\text{-}Cl)\}_8$(**A16**)$_4$(**A17**)$_8(\mu_2\text{-}Cl)_8]$. We consider this MOP with a cubic geometry with the BTC4A-based SBU as a 3-c node, although CIAC-108 can also be seen as a tetragonal prism from a different perspective.

4.4. Heterocube (cub-b)

MOPs with heterocube (binary cube) structures are comprised of two types of tritopic SBUs. In general, one of four kinds of inorganic SBUs located at the vertices is linked to four 3-c organic nodes. The cage shape resembles a face-capped tetrahedron, but topologically, we classified these MOPs as heterocubes, **cub-b**.

$[Fe_3O(SO_4)_3(py)_3]_4C_4$. A **cub-b**-MOP, MOP-54, was assembled from four $[Fe_3O(SO_4)_3(py_3)]$ SBUs, the same SBUs used to form **tet**-MOPs (IRMOP-50, -51, -52, -53), and four 1,3,5-benzenetribenzoate nodes, **C7** (Fig. 19).[15] MOP-54 ($[Fe_3O(SO_4)_3$-$(py)_3]_4$(**C7**)$_4$) exhibited permanent porosity and CO_2, CH_4, and benzene adsorption capacities.

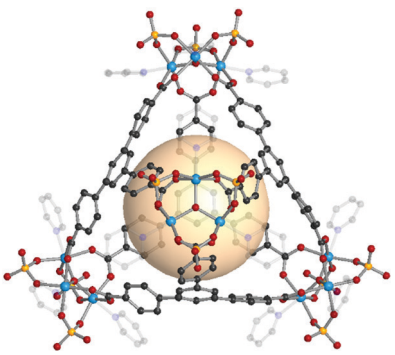

Fig. 19 Structural illustration of MOP-54, $[Fe_3O(SO_4)_3(py_3)]_4$(**C7**)$_4$.[15]

 This journal is © The Royal Society of Chemistry 2021

Published on 09 2020. Downloaded on 10/09/2024 14:36:19.

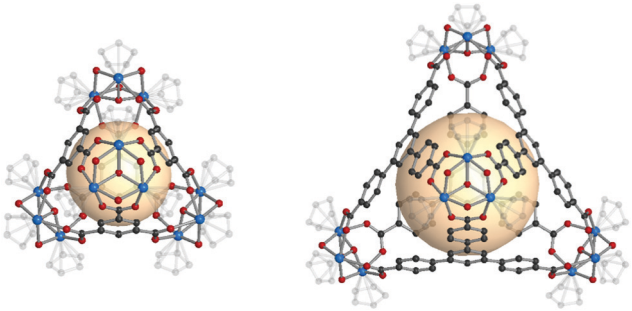

Fig. 20 Structural illustration of ZrT-2, $[Cp_3Zr_3O(OH)_3]_4$(**C1**)$_4$ (left) and ZrT-4, $[Cp_3Zr_3O(OH)_3]_4$(**C7**)$_4$ (right).[44]

$[Cp_3Zr_3O(OH)_3]_4C_4$. The **cub-b**-Zr-MOPs include four Zr clusters and four tritopic carboxylate linkers, $[Cp_3Zr_3O(OH)_3]_4C_4$. Two crystal structures of the heterocube cages have been reported, ZrT-2 ($[Cp_3Zr_3O(OH)_3]_4$(**C1**)$_4$) and ZrT-4 ($[Cp_3Zr_3O(OH)_3]_4$(**C7**)$_4$) with **C7** (Fig. 20).[44] Because the 3-c organic ligands observed in the single-crystal structures were relatively flat, the shape of the cages also can be considered to be tetrahedral with tritopic linkers on the faces. ZrT-2 and ZrT-4 are microporous. These MOPs exhibited stability in acetonitrile/water solutions under various pH conditions (2.2–9.8).[48]

$[V_6O_6(OCH_3)_9(SO_4)]_4C_4$. When the 3-c $[V_6O_6(OCH_3)_9(SO_4)]$ SBU was introduced to the tritopic organic ligands, **C1** and **C7**, the POV-based MOPs, VMOP-14 ($[V_6O_6(OCH_3)_9(SO_4)]_4$(**C1**)$_4$) and VMOP-15 ($[V_6O_6(OCH_3)_9(SO_4)]_4$(**C7**)$_4$), could be synthesized with heterocuboidal geometries (Fig. 21).[57] The molecular size of VMOP-15 was almost twice that of VMOP-14, due to the elongated tritopic linker, **C7**. Such isoreticular design for larger heterocubic **cub-b**-MOPs was utilized for selective adsorption of cationic dyes.[84] VMOP-18 and VMOP-19 were crystallized and synthesized by the coordination-driven assembly of the $[V_6O_6(OCH_3)_9X]$ cluster (X = VO_4 for VMOP-18; SO_4 for VMOP-19) and the tripotic 4,4′,4″-(1,3,5-triazine-2,4,6-triyl)tribenzoate (**C8**) node (Fig. 21). Their packing arrangement could be described as a body-centered cubic packing type. VMOP-18 exhibited highly selective adsorption of cationic dyes over neutral and anionic dyes in aqueous solutions, demonstrating the potential uses of POV-based MOPs.

$[M_4Cl(BTC4A)]_4C_4$. Liao *et al.* reported two heterecuboidal MOPs, $[Co_4Cl(BTC4A)]_4$(**C5**)$_4$ and $[Co_4Cl(BTC4A)]_4$(**C6**)$_4$, with calixarene-based SBUs.[85] The BTC4A-based SBU does not have a suitable geometry for tetrahedron-shaped cage formation because of its 4-connectivity. However, the asymmetrical **C5** linkers having one pyridyl and two carboxylate moieties produced heterocube MOPs. Each $[Co_4Cl(BTC4A)]$ was bridged by one pyridyl and two carboxylates from three different **C5** linkers. A fluorinated **C6** linker also formed the isostructural MOP. A vacant site in $[Co_4Cl(BTC4A)]$ was capped with formate.

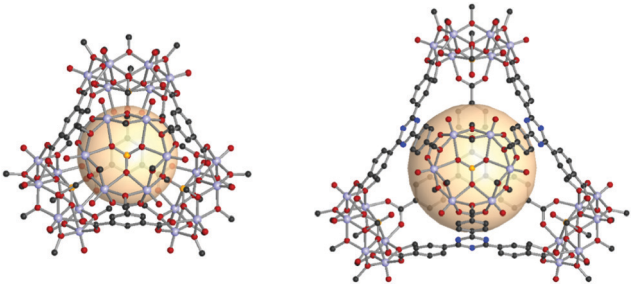

Fig. 21 Structural illustration of VMOP-14, $[V_6O_6(OCH_3)_9(SO_4)]_4$(**C1**)$_4$ (left)[57] and VMOP-19, $[V_6O_6(OCH_3)_9(SO_4)]_4$(**C8**)$_4$ (right).[84]

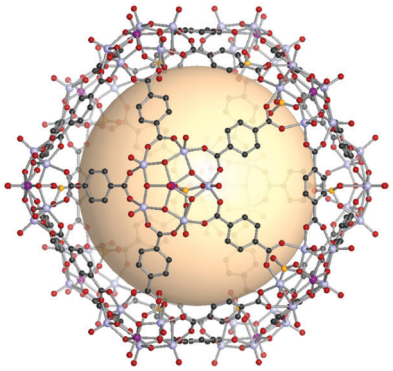

Fig. 22 Structural illustration of $[WV_5O_{11}SO_4]_{12}$(**A1**)$_{30}$.[86]

4.5. Icosahedron (ico)

An icosahedron belonging to one of five regular solids has 20 triangular faces, 30 edges, and 12 vertices. The RCSR three-letter code is **ico**. Icosahedral geometry is also found in virus capsid systems.[8] However, the artificial assembly of icosahedron-shaped coordination cages has been a daunting challenge due to the lack of accessible 5-c SBUs.[22] Recently, pentagonal-coordinated metal clusters have become available.

$[WV_5O_{11}(SO_4)]_{12}A_{30}$. Zaworotko *et al.* addressed the 5-c SBU, which contains the WV_5 polymetallic cluster, $[WV_5O_{11}(SO_4)]$.[86] The edge-directed assembly with 30 **A1** linkers yielded the elusive **ico** MOP, $[WV_5O_{11}(SO_4)]_{12}$(**A1**)$_{30}$, for the first time (Fig. 22). They also reported the isoreticular synthesis of larger **ico** MOPs using **A4** linkers, $[WV_5O_{11}(SO_4)]_{12}$(**A4**)$_{30}$.

5. Archimedean polyhedra

5.1. Cuboctahedron (cuo)

A cuboctahedron is a quasi-regular convex polyhedron composed of twelve vertices, twenty-four edges, and fourteen faces. More specifically, the faces consist of eight triangular faces and six square faces, each vertex is at the intersection between two triangular faces and two square faces, and each edge is at the intersection between a triangular face and a square face. The cuboctahedron is an Archimedean solid with octahedral symmetry (O_h). The RCSR letter code of a cuboctahedron is **cuo** with transitivity (1,1,2). The dual polyhedron of a cuboctahedron is a rhombic dodecahedron. To form a self-assembled cuboctahedron, twelve 4-c square planar SBUs at vertices and twenty-four bridging linkers between SBUs are needed. In this section, we introduce the cuboctahedral MOPs, assembled from twelve metal SBUs (M_2) and twenty-four bent

Published on 09 2020. Downloaded on 10/09/2024 14:36:19.

ditopic organic linkers (**B**) with 120° bond angles. Synthesized **cuo**-MOPs have the general formula of $(M_2)_{12}B_{24}$.

$(M_2)_{12}B_{24}$. A general procedure for synthesizing **cuo**-MOPs is to assemble M_2 SBUs and dicarboxylate linkers with 120° bond angles (Fig. 23). The nine paddlewheel M_2 accessible thus far are Cu_2, Mo_2, Cr_2, Ru_2, Rh_2, Ni_2, Pd–Cu, Pd–Ni, and Pd–Zn. The linkers of **cuo**-MOPs are mainly 5-R-1,3-benzenecarboxylic acid (R = functional group placed at the 5-position of a linker, such as H, OH, and Br; abbreviated 5-R-mBDC). In addition, 2,7-naphthalenecarboxylic acid (**H_2B54**) and 2,7-biphenylenedicarboxylic acid (**H_2B55**) can be used as linkers for **cuo**-MOPs. Table 3 shows representative examples of **cuo**-MOPs reported.

$(Cu_2)_{12}(B)_{24}$. As shown in Table 3, most **cuo**-MOPs have been comprised of Cu_2 SBUs. The Yaghi group synthesized a **cuo**-MOP using the Cu_2 node and **B14**.[11] The Zaworotko group also reported a hydroxylated Cu_2-based **cuo**-MOP with **B15**.[92] These hydroxylated **cuo**-MOPs have been used in applications such as a MOP precursor,[72] in composites with other materials,[97,106] or as supramolecular building blocks for MOFs.[93,95] McManus *et al.* synthesized a sulfonated Cu_2-based **cuo**-MOP with **B17**.[112] Because this particular **cuo**-MOP has a negative charge due to the functional groups of linkers, it can interact with positively charged species. The resulting compounds have a 3D porous network[113] and a 2D honeycomb architecture.[19] Banerjee and coworkers introduced three **cuo**-MOPs with the linkers **B22**, **B23**, and **B24**.[115] Because the linkers of **cuo**-MOPs are functionalized by alkoxy groups, the outer part of **cuo**-MOPs is more hydrophobic than the inner part of MOPs. When these **cuo**-MOPs were contacted with water, a hydrolytic conversion from MOP to MOF occurred, resulting in metal–organic nanosheets *via* self-exfoliation.

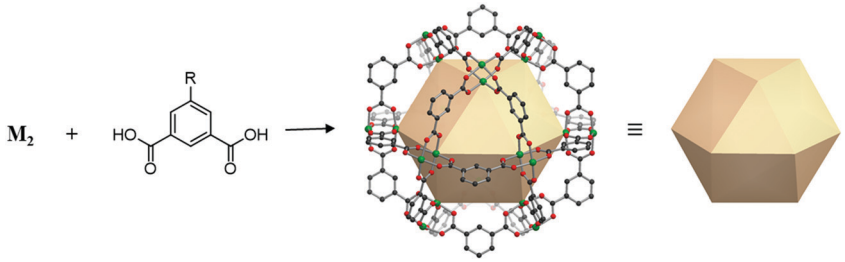

Fig. 23 Schematic illustration of the general design of **cuo**-MOPs with M_2 SBUs and 5-R-mBDC. M, green; C, black; O, red; all hydrogen atoms and solvents ligated on the metals are omitted for clarity.

Table 3 Examples of **cuo**-MOPs in the literature

Metal SBU	Linker	Ref.	Metal SBU	Linker	Ref.
Cu_2	**B14**	11, 72 and 87–91	Cu_2	**B53**	135
Cu_2	**B15**	72, 88, 92–95, 97 and 99–108	Cu_2	**B54**	109 and 136
Cu_2	**B16**	88, 101 and 109–111	Cu_2	**B55**	109
Cu_2	**B17**	19, 72, 100, 101, 105, 108, 112–114 and 116	Cu_2	**B14, B15**	72
Cu_2	**B18**	109	Cu_2	**B20, B47**	133
Cu_2	**B19**	88	Cu_2	**B20, B54**	72
Cu_2	**B20**	20, 72, 99–101, 105, 108, 117 and 118	Cu_2	**B15, B33**	137
Cu_2	**B21**	88	Mo_2	**B14**	73
Cu_2	**B22**	115	Mo_2	**B15**	73
Cu_2	**B23**	115 and 119	Mo_2	**B20**	73, 117 and 138
Cu_2	**B24**	115 and 119	Cr_2	**B14**	139
Cu_2	**B25**	109	Cr_2	**B15**	96
Cu_2	**B26**	98, 120 and 121	Cr_2	**B20**	96, 138 and 139
Cu_2	**B27**	122	Cr_2	**B44**	139
Cu_2	**B28**	118 and 123	Ru_2	**B14**	74
Cu_2	**B29**	118	Ru_2	**B20**	74 and 138
Cu_2	**B30**	21	Rh_2	**B14**	16 and 142
Cu_2	**B31**	119	Rh_2	**B15**	142
Cu_2	**B32**	119	Rh_2	**B34**	140 and 141
Cu_2	**B34**	17, 118 and 124–127	Rh_2	**B35**	141
Cu_2	**B40**	128	Rh_2	**B36**	143
Cu_2	**B42**	129	Rh_2	**B37**	143
Cu_2	**B43**	129	Rh_2	**B38**	142
Cu_2	**B44**	130 and 131	Rh_2	**B39**	142
Cu_2	**B45**	132	Rh_2	**B40**	143
Cu_2	**B46**	132	Rh_2	**B41**	143
Cu_2	**B48**	133	Ni_2	**B15**	76
Cu_2	**B49**	134	Pd–Cu	**B20**	144
Cu_2	**B50**	122	Pd–Ni	**B20**	144
Cu_2	**B51**	135	Pd–Zn	**B20**	144
Cu_2	**B52**	135			

 This journal is © The Royal Society of Chemistry 2021

Published on 09 2020. Downloaded on 10/09/2024 14:36:19.

Furukawa *et al.* synthesized a hydrophobic **cuo**-MOP with a dodecyloxy isophthalate linker, **B34**.[124] Due to the long alkyl chains of the linker, this **cuo**-MOP is hydrophobic and assembled as a form of diamond packing. Hosono and Kitagawa groups introduced two kinds of routes for synthesizing MOP-core star polymers, also known as coordination star polymers (CSPs).[129] **B42** and **B43** linkers, both of them functionalized by dithiobenzoate and trithioester chain transfer groups, respectively, were used to realize several CSPs with **cuo**-MOPs as cores.

$(Cu_2)_{12}(B^1)_n(B^2)_{24-n}$. The Zhou group synthesized **cuo**-MOPs with mixed linkers, the mixture of **B14** and **B15**, and the mixture of **B20** and **B54**.[72] 16 out of 24 **B15** linkers were exchanged with **B14** linkers *via* ligand substitution reaction in a solution of excess **B14** and the precursor **cuo**-MOP with **B15** by using the solubility of **cuo**-MOPs. A similar reaction, in a solution of excess **B54** as a larger sized linker and the precursor **cuo**-MOP with **B20**, substituted 12 **B54** linkers for 12 out of 24 **B20**. Park *et al.* synthesized a Cu_2-based **cuo**-MOP with a mixture of **B20** and **B47**.[133] This particular **cuo**-MOP was introduced as a stimulus-responsive MOP due to an azobenzene moiety in **B47**. Lal *et al.* synthesized the **cuo**-MOP with a mixture of **B15** with a hydrophilic moiety (–OH) and **B33** with a hydrophobic moiety ($-O(CH_2)_7CH_3$).[137] These two linkers were segregated in **cuo**-MOP like Janus particles. Due to the segregation of hydrophilic and hydrophobic parts, micellization by clustering of **cuo**-MOPs was observed through transmission electron microscopy (TEM).

$(Mo_2)_{12}(B)_{24}$. An essential advantage of MOPs with the Mo_2 node is that these MOPs can be studied in solution, unlike the Cu_2 counterparts.[73] The Zhou group synthesized a Mo_2-based **cuo**-MOP with the **B20** linker,[117] together with diverse quadruply-bonded Mo_2-based **cuo**-MOPs with **B14**, **B15**, and **B20** linkers.[73] Bloch *et al.* reported the optimized synthesis and activation of $(Mo_2)_{12}(\mathbf{B20})_{24}$.[138] This Mo_2-based **cuo**-MOP showed permanent porosity with the highest Brunauer–Emmett–Teller (BET) surface area (1321 $m^2\ g^{-1}$) among the reported MOPs. Compared to the synthesized iso-MOPs with Cr_2 and Ru_2 clusters, the BET surface area of $(Mo_2)_{12}(\mathbf{B20})_{24}$ was higher.

$(Cr_2)_{12}(B)_{24}$. The Zhou group synthesized several Cr_2-based **cuo**-MOPs with **B14**, **B20**, and **B44** linkers.[139] These Cr_2-based **cuo**-MOPs showed substantially higher gas uptake and surface area compared with the Cu_2 and Mo_2-based analogues. The Bloch group also reported Cr_2-based **cuo**-MOPs with **B15** or **B20** linkers,[96] and the latter **cuo**-MOP showed a high surface area and excellent N_2/O_2 selectivity.

$(Ru_2)_{12}(B)_{24}$. In many Cu_2 **cuo**-MOPs, the potential reactivity at the metal sites is rather limited. The redox-active nature of dinuclear Ru_2^{n+} species, however, is well-established with various oxidation states, ranging from tetra- to hexavalent. The Zhou group reported two Ru_2-based **cuo** MOPs with **B14** or **B20** with a Ru_2 redox-active core, while keeping their structural integrity.[74]

$(Rh_2)_{12}(B)_{24}$. The Furukawa group synthesized Rh_2-based **cuo**-MOPs with **B14**.[16] CO and NO molecules interacted strongly with Rh_2 centers and were trapped in **cuo**-MOPs. The Furukawa group also synthesized a Rh_2-based **cuo** MOP with **B34**.[140] Kawano *et al.* synthesized Rh_2-based **cuo**-MOPs with **B34** or **B35**.[141] Both functionalities placed at the 5-position of the linkers were long alkyl chains, and therefore, these MOPs exhibited good solubility in lipid bilayers through hydrophobic interactions. In general, Rh-based MOPs are robust with high thermal and chemical stability. Carné-Sánchez *et al.* further investigated the functionalization of Rh-based MOPs with **B15**. Through post-synthetic modification, hydroxyl groups of the MOP reacted with acyl anhydrides and chlorides to form MOPs with acetate ester and acrylate ester groups (**B38** and **B39**).[142] A recent work by Maspoch and coworkers showed a Rh_2 **cuo**-MOP with carboxylic acid groups at the 5-position of the linkers (**B37**).[143] While the 1,3,5-benzenetricarboxylic acid (**B37**) linker often produced extended coordination networks, the protecting group (in **B36**) was employed and later removed for the synthesis of the MOP. Similar protection and removal were conducted to obtain the amino **B16**-based MOP from protected **B41** linkers.

$(Ni_2)_{12}(B)_{24}$. A Ni_2-based **cuo**-MOP can be assembled with the linker **B15**.[76] It is well-established that the first-row transition metal cations can be easily incorporated into M_2 SBUs. For example, the metal cations from Cr^{2+} to Zn^{2+} form MOFs with M_2 SBUs. The effort to access **cuo** MOPs with a new combination of M_2 SBUs possibly offers a new opportunity to control porosity, stability, and catalytic properties.

$(M\text{-}Pd)_{12}(B)_{24}$. Sumby and Doonan groups reported **cuo**-MOPs, assembled from the **B20** linker and heterobimetallic M–Pd, where M = Cu, Ni, or Zn.[144] Interestingly, Pd(II) was predominantly localized at the inner nodes. These heterobimetallic MOPs exhibited exceptionally high H_2 uptake and binding affinities for H_2.

An isoreticular series of **cuo**-MOPs is possible, as shown in Fig. 24. As the size of the linker grows, the resulting **cuo**-MOPs get larger, while keeping the cuboctahedral geometry, as exemplified by MOP-23 and MOP-24 with the linkers **B54** and **B55**, respectively.[109]

6. Catalan polyhedra

6.1. Rhombic dodecahedron (rdo)

A rhombic dodecahedron, classified as a Catalan solid, is the dual of a cuboctahedron. Twelve rhombus faces form a rhombic dodecahedron. The transitivity is (2,1,1), and there are two types of vertices: six of the 4-c and eight of the 3-c nodes. The RCSR letter code of the rhombic dodecahedron is **rdo**. The combination of different 4-c and 3-c metal-cluster SBUs might be difficult in molecular polyhedron synthesis. In **rdo**-MOP assembly, metal-cluster SBUs are used as 4-c nodes, and the branching point of tritopic organic linkers is used as the 3-c node. Specifically, **rdo**-MOPs are assembled when six 4-c SBUs meet eight 3-c organic linkers.

$[V_4O_8Cl]_6C_8$ and $[V_5O_9Cl]_6C_8$. Polyhedron-shaped molecular cages with POVs and organic ligands were reported by

Published on 09 2020. Downloaded on 10/09/2024 14:36:19.

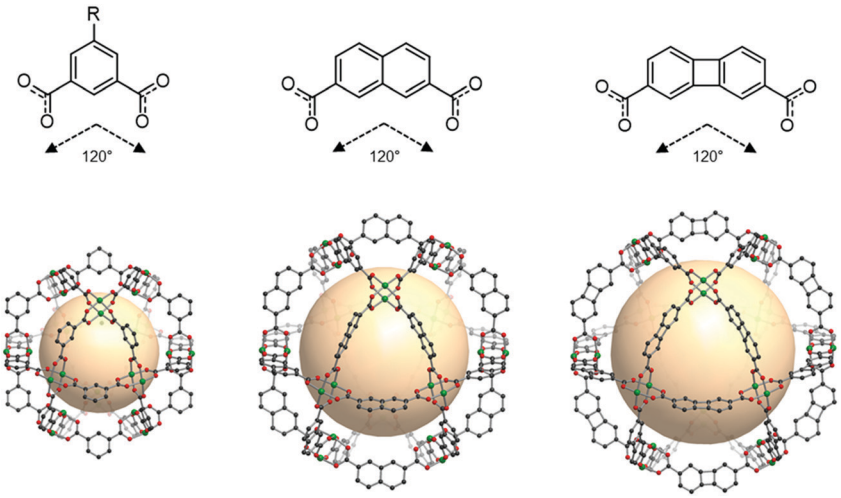

Fig. 24 Chemical diagrams of 5-R-1,3-benzenedicarboxylate, **B54**, and **B55** linkers, which have 120° bond angles. Structural illustration of **cuo**-MOPs resulting from the combination of M_2 nodes and each linker.[72,109]

Zaworotko *et al.*[145] Six shuttlecock-shaped POV clusters ([V_4O_8Cl] or [V_5O_9Cl]) as a 4-c node and eight tritopic carboxylate linkers, **C1**, formed small rhombic dodecahedral nanoballs. Different synthesis conditions and solvents afforded hyball-3, [V_4O_8Cl]$_6$(**C1**)$_8$, and hyball-4, [V_5O_9Cl]$_6$(**C1**)$_8$, with the same molecular octahedral geometries (Fig. 25). After exposure to the atmosphere for two weeks, the packing of hyball-3 was rearranged to hyball-3′ with additional hydrogen bonding around the [NH_2Me_2]$^+$ cation. The resulting network was a doubly interpenetrated **pcu** net, which is another example of POV-based MOPs as supramolecular building blocks for the porous network. Hyball-4 was composed of pentanuclear [V_5O_9Cl] clusters, and a V^{5+} cation was located above four square pyramidal V^{4+} cations.

[M_4Cl(BTC4A)]$_6C_8$ and [M_4O(TBSC)]$_6C_8$. Attractive calixarene-based rhombic dodecahedral nanocages were assembled from [Co_4(calix)(μ_4-Cl)] (calix = BTC4A or deprotonated *p*-phenylthiacalix[4]arene (H_4PTC4A)) as a 4-c node and a **C1** (or **C7**) tritopic organic linker as a 3-c node.[146] Four **rdo** coordination cages, CIAC-101 ([Co_4(BTC4A)Cl]$_6$(**C1**)$_8$), CIAC-102 ([Co_4(PTC4A)Cl]$_6$(**C1**)$_8$), CIAC-103 ([Co_4(BTC4A)Cl]$_6$(**C7**)$_8$), and CIAC-104 ([Co_4(PTC4A)Cl]$_6$(**C7**)$_8$), were created with different cage sizes (Fig. 26). The internal cavity sizes vary from 1.1 nm for CIAC-101 and -102 to 1.7 nm for CIAC-103 and -104. The tritopic linkers **C1** and **C7** capped the faces of the octahedron, and 4-c calixarene-based SBUs were located on the vertices of the octahedron. These MOPs can be assigned as **rdo** polyhedra with 4-c and 3-c nodes.

A similar calixarene-based 4-c SBU, [M_4(TBSC)(μ_4-H_2O)], can be used for the assembly of rhombic dodecahedron-shaped MOPs with tritopic organic linkers. Wang *et al.* introduced a modular assembly of **rdo** coordination cages using various sulfonylcalix[4]arenes, metals, and organic linkers.[147] MOSC-1-M (M = Ni, Co, Mg), a ([M_4(TBSC)(μ_4-H_2O)]$_6$(**C1**)$_8$) series, was reported first. The modular aspect of the synthesis was proven to be successful as can be seen in MOSC-2-Ni ([Ni_4(DTBSC)(μ_4-H_2O)]$_6$(**C1**)$_8$), de-*p*-*tert*-butylsulfonylcalix[4]arene (H_4DTBSC), MOSC-3-Co ([M_4(DTBSC)(μ_4-H_2O)]$_6$(**C2**)$_8$), and MOSC-4-Co ([M_4(TBSC)(μ_4-H_2O)]$_6$(**C7**)$_8$). Liao *et al.* synthesized the two giant **rdo** coordination cages, CIAC-107 and CIAC-114, [Co_4(TBSC)(OH)]$_6$(**C9**)$_8$[148] and [Co_4(TBSC)(OH)]$_6$(**C10**)$_8$,[149] exhibiting an astonishing size of 5.0 nm and 5.4 nm, respectively. The reaction with [M_4(TBSC)(μ_4-H_2O)] (M = Ni and Co) and the

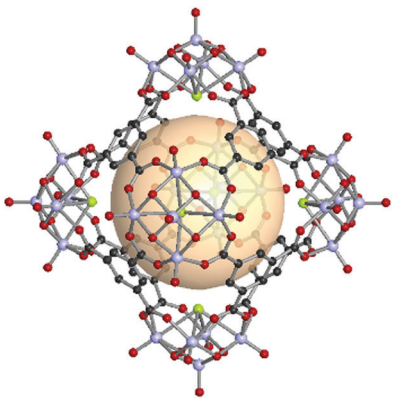

Fig. 25 Structural illustration of hyball-4, [(V_5O_9Cl)$_6$(**C1**)$_8$].[145]

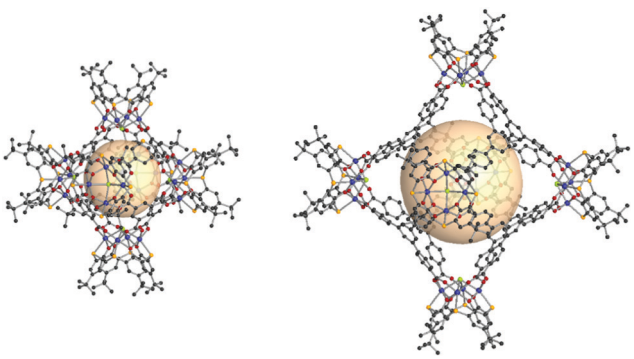

Fig. 26 Structural illustration of CIAC-101 (left) and CIAC-103 (right), [Co_4(BTC4A)Cl]$_6$(**C1**)$_8$ and [Co_4(BTC4A)Cl]$_6$(**C7**)$_8$, respectively.[146]

 This journal is © The Royal Society of Chemistry 2021

Published on 09 2020. Downloaded on 10/09/2024 14:36:19.

enantiopure **C11** linker produced the chiral and catalytically active **rdo**-MOP, $[M_4(TBSC)(\mu_4\text{-}H_2O)]_6(\mathbf{C11})_8$.[150] Three carboxylate moieties in the phosphoric acid-containing spiro ligand, **C11**, were bridged to the $[M_4(TBSC)(\mu_4\text{-}H_2O)]$ SBU. Some of the dangling carboxylates, which do not make coordination bonding, formed intercage hydrogen bonding with phosphoric acid in the adjacent cage. Due to the asymmetrical linker shape, the **rdo**-MOP had an elongated molecular shape. The exposed phosphoric acid as the strong Brønsted acid groups acted as an efficient asymmetric catalyst.

$(M_2)_6C_8$. To form a rhombic dodecahedral MOP using an M_2 paddlewheel SBU, the 3-c node component, *i.e.*, the tritopic organic linkers, should be flexible and non-planar. The Lah group initiated the M_2-based **rdo**-MOP assembly using the **C16** 3-c organic node.[151] The **rdo**-MOP formula was $(Cu_2)_6(\mathbf{C16})_8$ (Fig. 27). Meta-positioned carboxylates which formed coordination bonding with Cu_2 were perpendicular to the central phenyl ring assigned as a 3-c node. The smallest-sized **rdo**-MOP was synthesized using a Cu_2 SBU and **C12**.[152] When the **C12** linker had a *syn–syn–syn* conformation with the same carboxylate direction, the **rdo**-MOP could be formed. Liang *et al.* reported a **rdo**-MOP with Cu_2 and the L-alanine-derived tritopic linker, **C13**.[153] The synthesized $(Cu_2)_6(\mathbf{C13})_8$ MOP had the same amide moiety in the organic linker as the $(Cu_2)_6(\mathbf{C16})_8$ MOP, except for the size of the linkers. An example of nearly ideal **rdo**-shaped MOP $(Cu_2)_6(\mathbf{C15})_8$ was reported.[154] The molecular geometry of phenoxymethyl in the **C15** linker is suitable to arrange nearly perpendicular to the central phenyl ring, preventing distortion of the **rdo**-MOP. A smaller tritopic linker (**C14**) was utilized by Huang *et al.* and a similar **rdo** MOP was reported.[155]

6.2. Rhombic triacontahedron (trc)

The rhombic triacontahedron is the most common thirty-faced polyhedron, containing thirty rhombus faces, sixty edges, and thirty-two vertices. The rhombic triacontahedron has the RCSR code **trc**. The **trc**-MOPs are comprised of two types of vertices, twelve 5-c SBUs and twenty 3-c organic nodes. Similar to the icosahedron, the 5-c SBU is exceptionally scarce. There is an example of an ideal **trc**-MOP.[86] Another case is a **trc**-MOP with two missing organic nodes.[156]

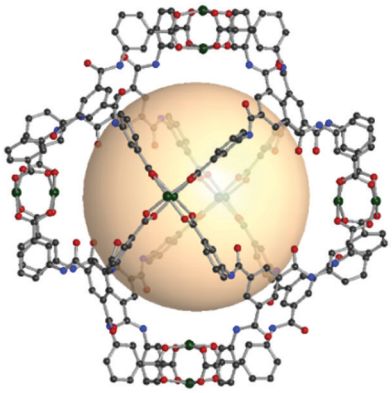

Fig. 27 Structural illustration of $[(Cu_2)_6(\mathbf{C16})_8]$.[151]

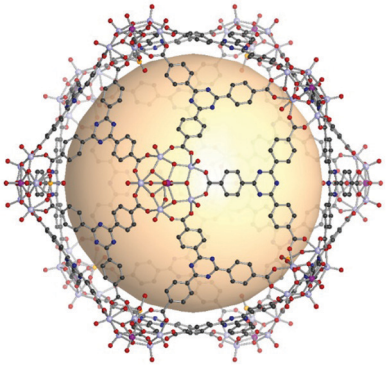

Fig. 28 Structural illustration of $[WV_5O_{11}(SO_4)]_{12}(\mathbf{C8})_{20}$.[86]

$[WV_5O_{11}(SO_4)]_{12}C_{20}$. Ideal **trc**-MOP assemblies were formed by a combination of twelve 5-c $[WV_5O_{11}(SO_4)]$ SBUs and twenty tritopic linkers as the 3-c nodes, **C1** and **C8**.[86] The formula of assembled **trc**-MOPs was $[WV_5O_{11}(SO_4)]_{12}(\mathbf{C1})_{20}$ and $[WV_5O_{11}(SO_4)]_{12}(\mathbf{C8})_{20}$. The molecular size of $[WV_5O_{11}(SO_4)]_{12}(\mathbf{C8})_{20}$ was about 4.3 nm (Fig. 28). Thirty-two node components are the largest number in MOP assemblies.

$[M_4Cl(BTC4A)]_{12}C_{18}$. Zheng *et al.* reported a **trc**-MOP with two missing 3-c nodes formed from the asymmetric tritopic linker, **C3**.[156] The SBU used, $[M_4Cl(BTC4A)]$, typically acts as a 4-c node, but with the asymmetric **C3** linker, six of the $[M_4Cl(BTC4A)]$ SBUs act as 5-c nodes (Fig. 29). Interestingly, two of the cofacial 3-c nodes were missing in $[M_4Cl(BTC4A)]_{12}(\mathbf{C3})_{18}$. Six of SBUs were 5-c nodes, and the other six SBUs near the defect sites became 4-c nodes.

7. Semi-regular polyhedra

7.1. Triangular prism (trp)

A triangular prism is composed of two triangles on the top and bottom faces and three rectangles on the side with D_{3h} symmetry. The right prismatic polyhedra are semi-regular solids of (1,2,2) transitivity. The RCSR code is **trp**. There is only one example of a **trp**-MOP structure in the literature.

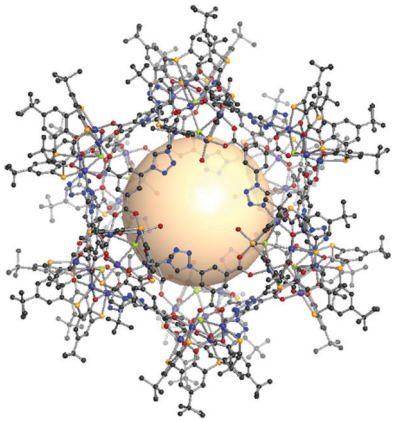

Fig. 29 Structural illustration of $[M_4Cl(BTC4A)]_{12}(\mathbf{C3})_{18}$.[156]

Published on 09 2020. Downloaded on 10/09/2024 14:36:19.

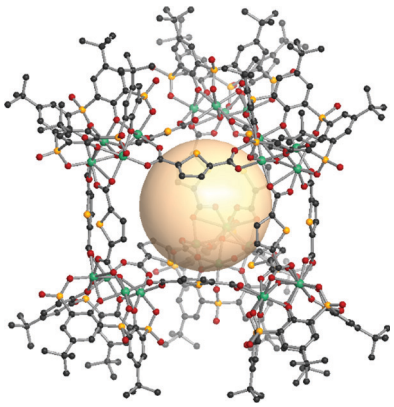

Fig. 30 Structural illustration of $[Ni_4O(TBSC)]_6$(**B58**)$_{12}$.[158]

$[Ni_4O(TBSC)]_6(B)_6(B_2)_3$. Chen *et al.* reported the **trp**-MOP, $[Ni_4O(TBSC)]_6$(**B58**)$_{12}$ (Fig. 30).[157,158] The cluster $[Ni_4O(TBSC)]$ is generally known as a 4-c SBU. However, in the **trp** case, it became a 3-c node. The edge description was different, unlike other edge-transitive MOPs because doubly bridging **B58** linkers corresponded to the three edges on the sides of the rectangle. The bent geometry of the thiophene of the **B58** linker formed a triangular prismatic cage. Four carboxylates of the linkers formed coordination bonds with $[Ni_4O(TBSC)]$, but two of them on the side were considered to be one edge of the **trp**-MOP.

8. Other miscellaneous polyhedra

8.1. Anticuboctahedron (twc)

A anticuboctahedron is similar to the cuboctahedron but distinctly different. Imagine separating a cuboctahedron into two upper and lower parts (Fig. 31). Rotation of the lower part by 180°, followed by joining two parts, creates an anticuboctahedron. While a cuboctahedron belongs to an Archimedean solid, an anticuboctahedron is a Johnson solid, often referred as a triangular orthobicupola, J_{27}. The RCSR code for an anticuboctahedron is **twc** with transitivity (2,4,3), named after a twinned cuboctahedron.

$[M_2]_{12}B_{24}$. The **twc** MOP can be considered as a structural isomer of the **cuo**-MOP. The **twc**-MOP was synthesized from paddlewheel Cu_2 units and **B22** linkers.[112] Apparently, the square face connectivity was different from that of the typical **cuo**-MOP. Another **twc** M_2 MOP was synthesized from a Mo_2 unit and the **B14** linker.[117] Zhou *et al.* also synthesized an extended **twc**-MOP cage using a larger bent-type linker (**B54**), $(Mo_2)_{12}$(**B54**)$_{24}$.[73] A Rh_2-based anticuboctahedral MOP was reported by Kitagawa *et al.*[16] The $(Rh_2)_{12}$(**B14**)$_{24}$ **twc**-MOP possessed a higher gas (N_2 and CO) adsorption capacity compared to that of Cu_2-based **cuo**-MOPs.

8.2. Hendecahedron (mtq-d)

A hendecahedron is a polyhedron with 11 faces, and numerous topologically different isomers are possible. In the molecular assembly, an odd number of faces and vertices is significantly rare. Surprisingly, Zhou *et al.* successfully demonstrated the assembly of metal–organic hendecahedra with an odd number of faces and vertices with **mtq-d** topology with transitivity (2,2,3).[159] The dual of **mtq** topology is **mtq-d**.[160]

$[M_2]_9(B')_6(B'')_{12}$. The construction of **mtq-d** MOPs was made by mixing two types of bent angle linkers, 90° and 120°, together with 4-c Cu_2 SBUs.[159] The linkers used were **B4** (90°) and **B56** (120°) and **B57** (120°). The **mtq-d**-MOPs, $(Cu_2)_9$(**B4**)$_6$(**B56**)$_{12}$ and $(Cu_2)_9$(**B4**)$_6$(**B57**)$_{12}$, are comprised of six **B4** linkers and twelve **B56** or **B57** linkers (Fig. 32). The twelve 120° linkers, **B56** or **B57**, form polygons on the sides.

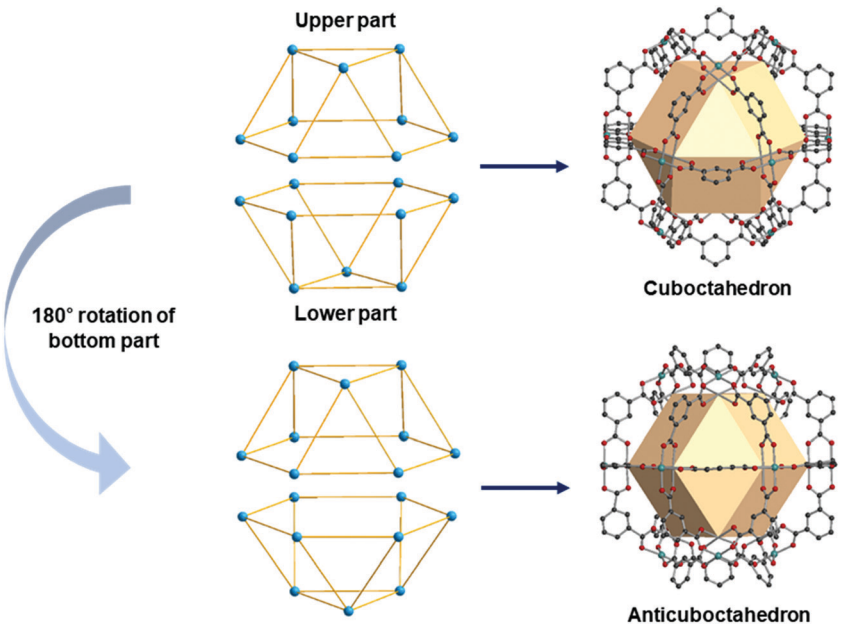

Fig. 31 Schematic representation of the differences between a cuboctahedron and an anticuboctahedron.

 This journal is © The Royal Society of Chemistry 2021

Published on 09 2020. Downloaded on 10/09/2024 14:36:19.

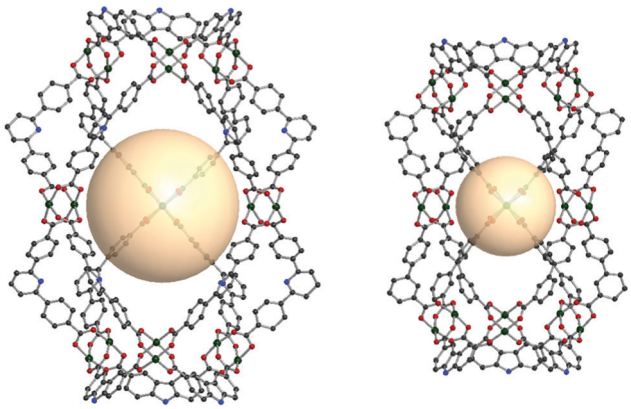

Fig. 32 Structural illustration of $(Cu_2)_9$(**B4**)$_6$(**B56**)$_{12}$ (left) and $(Cu_2)_9$-(**B4**)$_6$(**B57**)$_{12}$ (right).[159]

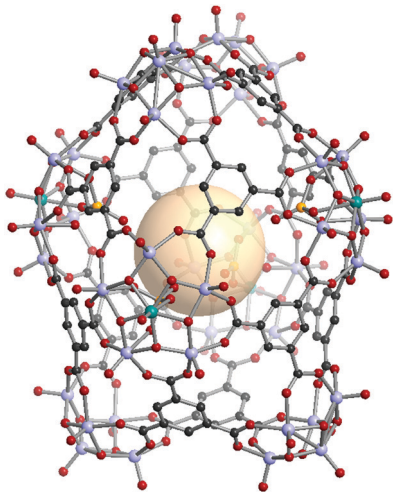

Fig. 33 Structural illustration of VMOP-22, $\{[V_5O_9(OCH_3)]_4[MoV_5O_{11}(SO_4)]_4\}$(**C1**)$_{12}$.[161]

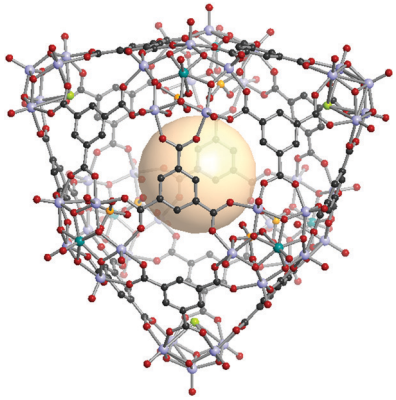

Fig. 34 Structural illustration of VMOP-23, $\{[V_5O_9Cl]_3[MoV_5O_{11}(SO_4)]_6\}$-(**C1**)$_{14}$.[161]

8.3. Metal–organic Johnson deltahedra

A deltahedron is a polyhedron with equilateral triangular faces. There are eight convex deltahedra. The other five deltahedra belong to Jonson solids and they are called Johnson deltahedra, including triangular bipyramid (**tbp**), pentagonal bipyramid (**ppi**), snub disphenoid (**bds**), triaugmented triangular prism (**tct**), and gyroelongated square bipyramid (**csa**). Deltahedral geometries are well known in the main group and coordination chemistry, such as *closo*-carboranes and inorganic coordination complexes. Three types of geometries (**bds**, **tct**, **csa**) were assembled with new metal–organic Johnson deltahedra as their face-capped topologies (**ghm**, **hmg**, **xum**, respectively) by using the combination of 4-c and 5-c SBUs.[161,162]

8.3.1. Face-capped snub disphenoid (ghm). The snub disphenoid (**bds**), one of the Johnson solids (J_{84}), has 12 triangular faces and 8 vertices. It is a common geometry in coordination compounds, also known as "bisdisphenoid". Wang *et al.* synthesized a face-capped snub disphenoid (**ghm**) type MOP, VMOP-22.[161]

$[V_5O_9(OCH_3)]_4[MoV_5O_{11}(SO_4)]_4C_{12}$. VMOP-22 are composed of four 4-c SBUs ($[V_5O_9(OCH_3)]$), four 5-c SBUs ($[MoV_5O_{11}(SO_4)]$) and twelve **C1** linkers. The overall formula of VMOP-22 is $\{[V_5O_9(OCH_3)]_4[MoV_5O_{11}(SO_4)]_4\}$(**C1**)$_{12}$ (Fig. 33).

8.3.2. Face-capped triaugmented triangular prism (hmg). The triaugmented triangular prism (**tct**) is one of the Johnson solids known as J_{51} and has fourteen triangular faces and nine vertices. It is a well-known coordination geometry as the "tricapped trigonal prismatic molecular geometry", a common feature in nona-coordinating complexes. A MOP with face-capped triaugmented triangular prism (**hmg**) topology, VMOP-23, was synthesized by Wang *et al.*[161]

$[V_5O_9Cl]_3[MoV_5O_{11}(SO_4)]_6C_{14}$. Three 4-c $[V_5O_9Cl]$ and six 5-c $[MoV_5O_{11}(SO_4)]$ clusters are located on the nine vertices of the **tct** polyhedron. Fourteen 3-c **C1** linkers connected these SBUs to assemble **hmg** MOP, VMOP-23 (Fig. 34). The overall formula of VMOP-23 is $\{[V_5O_9Cl]_3[MoV_5O_{11}(SO_4)]_6\}$(**C1**)$_{14}$.

8.3.3. Face-capped gyroelongated square bipyramid (xum). A hexadecahedron with 16 faces has numerous topologically different isomers. Xu *et al.* and Hang *et al.* reported face-capped gyroelongated square bipyramidal MOPs.[161,162] The arrangement of 10 SBUs in the vertices indicated the gyroelongated square bipyramid geometry, known as the Johnson-type solid J_{17} with **csa** topology, according to the RCSR code. However, the linker used to cap the 16 triangular faces was the tritopic **C1** or **C4**, as a 3-c node. The topological code was **xum** from the RCSR. However, we could not find the exact name for this polyhedron.

$[V_5O_8(CN)_2]_2[V_6O_{11}(SO_4)]_8C_{16}$. Two $[V_5O_8(CN)_2]$ SUBs as a 4-c node and eight $[V_6O_{11}(SO_4)]$ SBUs as a 5-c node are assembled with sixteen face-capping 3-c **C1** organic linkers to form VMOP-24 with **xum** topology.[161] The overall formula of VMOP-24 is $\{[V_5O_8(CN)_2]_2[V_6O_{11}(SO_4)]_8\}$(**C1**)$_{16}$ (Fig. 35).

$\{[M_4(BTC4A)]_{10}Cl_6X_4\}C_{16}$ (X = CO_3, HCOO, MeNCOO, or HC4). In this structure, there are three kinds of nodes.[162] Two of them are $[Ni_4(BTC4A)]$ SBUs, utilized as 4-c or 5-c nodes, and the remaining one is **C4**, the 3-c asymmetric organic linker. The 4-c $[Ni_4Cl(BTC4A)]$ SBUs are located on top and bottom of the polyhedron, and four carboxylates of **C4** are coordinated to the Ni_4 cluster. The other eight $[Ni_4(BTC4A)]$ SBUs are nodes, but four of them have different coordination environments of the Ni_4

Published on 09 2020. Downloaded on 10/09/2024 14:36:19.

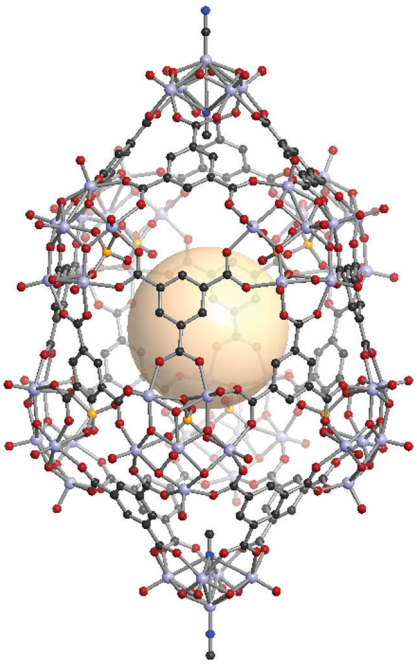

Fig. 35 Structural illustration of VMOP-24, $\{[V_5O_9(CN)_2]_2[V_6O_{11}(SO_4)]_8\}$-(**C1**)$_{16}$.[161]

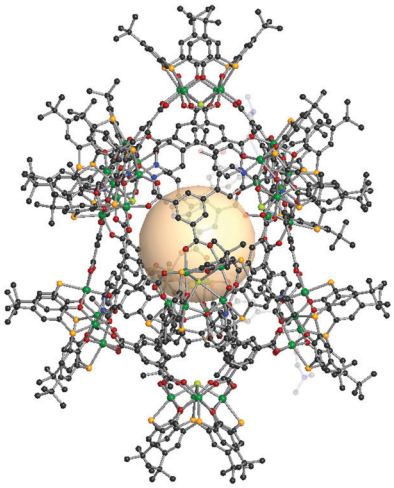

Fig. 36 Structural illustration of $\{[M_4(BTC4A)]_{10}Cl_6X_4\}$(**C4**)$_{16}$.[162]

cluster, compared to the chloride-coordinated $[Ni_4Cl(BTC4A)]$. The different types of anions, denoted as X, are coordinated in a disordered fashion to the Ni_4 cluster instead of Cl. The overall formula for **xum** MOP is $\{[M_4(BTC4A)]_{10}Cl_6X_4\}$(**C4**)$_{16}$ (Fig. 36).

9. Notable polyhedra without metal-cluster SBUs

9.1. Coordination-driven self-assembly for Goldberg polyhedra

Some coordination cages built from Pd cations and pyridyl linkers are worthy of mention in this review, bridging the gap between MOPs and coordination cages. Perhaps MOF chemists can gain significant insights from these extraordinary cages made by Fujita and others. The cage with **rdo** topology, $[Pd_6(C_{24}H_{21}N_3)_8]^{12+}$, was prepared with six Pd atoms and eight tridentate ligands ($C_{24}H_{21}N_3$ = 1,3,5-tris(4-pyridylmethyl)-benzene) (Fig. 37).[163] The Pd atoms are located at the vertices of the octahedron. Each Pd cations form a square planar geometry with four coordinated pyridyl groups of the ligands. Yaghi and coworkers reported Pd-based **rdo** cages, MOP-100 and MOP-101, composed of tetrakis(1-imidazolyl)borate and tetrakis(4-methyl-1-imidazolyl)borate linkers, respectively.[164] Two **cuo** cages by Fujita and coworkers, $[Pd_{12}(C_{14}OH_{10}N_2)_{24}]^{24+}$ and $[Pt_{12}(C_{14}OH_{10}N_2)_{24}]^{24+}$, were synthesized with ditopic pyridyl ligands ($C_{14}OH_{10}N_2$ = 2,5-bis(4-pyridyl)furan) (Fig. 37).[165,166] By utilizing functionalized ligands, the inner or outer space of the **cuo** cage was tuned with various organic moieties.[167] One of the interesting approaches showed the attachment of the other pyridyl ligand moieties in the precursor ligands, resulting in sphere-in-sphere complexes.[168] When the ligand ($C_{14}SH_{10}N_2$ = 2,5-bis-(4-pyridyl)thiophene) with a larger bent angle was used, a larger coordination cage, $[Pd_{24}(C_{14}SH_{10}N_2)_{48}]^{48+}$ with **rco** (rhombicuboctahedron) geometry, was formed (Fig. 37).[169] The next extension of the M_nL_{2n} series, $M_{30}L_{60}$ with the **ido** geometry, was prepared with a longer thiophene-cored bipyridyl linker, resulting in a giant cage with a size up to 8 nm (Fig. 37).[170]

Out of the regular and semi-regular polyhedra, Goldberg polyhedra composed of triangles and squares were synthesized, with the formulas $M_{30}L_{60}$ and $M_{48}L_{96}$, which had not been previously reported at the molecular level.[171] To form $M_{30}L_{60}$ and $M_{48}L_{96}$ structures, a selenophene-cored bipyridyl linker with a slightly larger bend angle than that of the thiophene-cored linker was used, forming a rhombicuboctahedral cage (Fig. 37). With the same selenophene-cored linker, $M_{48}L_{96}$ was prepared. Self-assembly of giant polyhedra, from large numbers of small components, might be the state-of-the-art in supramolecular chemistry,[170–172] which reminds us of the polyhedral protein complexes.[173–175]

9.2. Coordination cages with organic SBUs

Recently, intriguing calixarene assemblies were emerged with calix[*n*]arenes, acting as *n*-c nodes. On the other hand, these calix[*n*]arenes could be defined as a core with *n* number of 3-c nodes (center of the phenyl ring; two for adjacent phenyl, and one for the coordination center), unlike metal-cluster based SBUs which we have covered in this review.[38]

Some examples show coordination cages, including macrocyclic compounds such as pyrogallolarene and calixarene. The Atwood group reported an octahedral cage ($Cu_{24}(Pg)_6$, Pg = *C*-propan-3-ol pyrogallol[4]arene) (Fig. 38).[176] In the structure, Pg SBUs were located at the vertices of the octahedron, and three copper ions formed coordination bonds with the linkers on each face of the octahedron. Considering the copper ions as building units with three connectivity, the cage can be interpreted as a **rdo**-type cage. Strictly speaking, the topology of the $Cu_{24}(Pg)_6$ cage is a **rdo**-derived **tro** (*i.e.* truncated octahedron), when Pg is considered to be a square with four 3-c nodes.

 This journal is © The Royal Society of Chemistry 2021

Published on 09 2020. Downloaded on 10/09/2024 14:36:19.

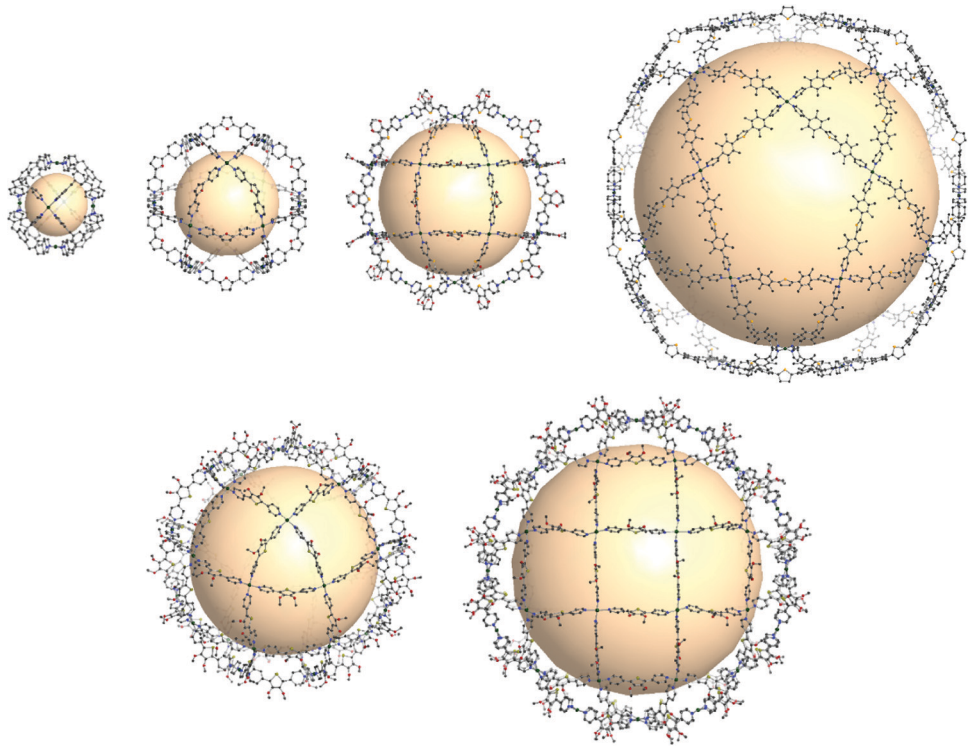

Fig. 37 Structural illustration of coordination cages composed of Pd ions and bipyridyl linkers. Examples of **rdo-**, **cuo-**, **rco-**, and **ido-**type cages (first row). Cages with the formulas $M_{30}L_{60}$ and $M_{48}L_{96}$ corresponding to Goldberg polyhedra (second row).[163–171]

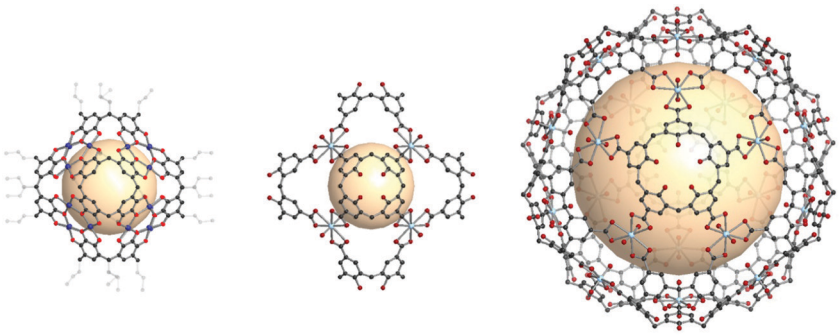

Fig. 38 Structural illustration of coordination cages, including macrocyclic compounds. A **rdo**-derived **tro-**type cage synthesized with pyrogallol[4]arene linkers (left). Cages composed of calixarene linkers and uranyl ions showing **rdo-**derived **tro** and **trc**-derived **deg** topologies (middle and right).[176,182]

With various metal ions, similar cages were synthesized, showing control over the coordination geometry of the metal ions.[176–181]

Other macrocyclic compounds, calix[4]arene tetracarboxylate (CTC) and calix[5]arene pentacarboxylate (CPC), were employed to construct coordination cages with uranyl (UO_2^{2+}) ions.[182] In the case of CTC, a cage with **rdo**-derived **tro** topology, $[(UO_2)_8(CTC)_6]^{8-}$, was synthesized with six CTCs on the vertices and eight 3-c uranyl (UO_2) nodes (Fig. 38). When CPC linkers were used, a combination of the linkers with five connectivity and uranyl nodes with three connectivity resulted in a cage with a **trc**-derived **deg** topology, $[(UO_2)_{20}(CPC)_{12}]^{20-}$ (Fig. 38). What is striking here is the five-fold symmetry of CPC, making it possible to build a **trc** with 12 pentagon faces. Introducing the five-fold symmetry nodeis an important contribution because it can lead to exotic polyhedra (*e.g.*, **ico**, **ido**) with five-fold symmetry.

Cotton *et al.* reported a **tet** cage assembled from four 3-c organic SBUs with 120° coordination bond angles and six inorganic linkers as edges (Fig. 39).[183] Topologically, organic and inorganic building blocks are used as nodes and linkers, respectively, unlike typical MOPs assembled from inorganic nodes and organic linkers. The organic SBU, **C1**, was linked with 2-c Mo_2 paddle wheel linkers, and adjacent carboxylate units were bridged. The 2-c Mo_2 linker had a 90° linkage angle. Two non-bridging coordination sites on the Mo_2 paddle wheel

Published on 09 2020. Downloaded on 10/09/2024 14:36:19.

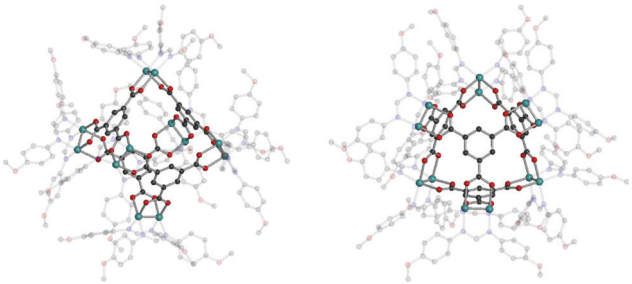

Fig. 39 Structural illustrations of (**C1**)$_4$[Mo$_2$(DAniF)$_2$]$_6$.[183]

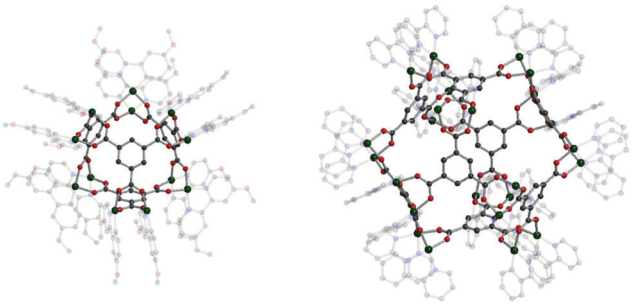

Fig. 40 Structural illustration of (**C1**)$_4$[Cu$_2$(OMe-bipy)$_2$]$_6$ (left) and (**C1**)$_8$[Cu$_2$(bipy)$_2$]$_{12}$ (right).[186]

were capped by two *N*,*N*′-di-*p*-anisylfromamidinate (DAniF) anions. An isostructural **tet** cage can be made with the Rh$_2$ node, in addition to the Mo$_2$ dimer.[184] The combination of M$_2$ inorganic linkers and other well-designed organic SBUs might afford new polyhedral structures.[185] After 20 years, Bloch *et al.* synthesized **tet** and **cub** cages based on 2-c Cu$_2$ paddle wheel linkers and **C1** as the organic SBU (Fig. 40).[186] Cu paddle wheels in **tet** and **cub** cages were capped by two bipyridines (2,2′-bipyridine (bipy) for **cub** and 4,4′-dimethoxy bipy (OMe-bipy) for the **tet** cage). Indeed, there are more chances to make unique polyhedral architectures using a variation of the combination of SBU and linkers.

10. Concluding remarks and future perspectives

After the first appearance of Cu-based MOP in 2001, the reticular design of MOPs, assisted by topological guidance, has been popular as exemplified by the MOPs with 14 topologies (including nine edge-transitive ones) highlighted in this review. In addition to such symmetrically pleasing topologies, rather limited applications are suggested for MOPs, unlike MOFs. The fact that MOPs are significantly under-explored probably stems from chemical stability and permanent porosity. Creating highly porous MOPs has been a challenge for MOP community. MOPs with over 1000 m^2 g^{-1} of BET surface area are quite recent works, including a BET surface area of 1321 m^2 g^{-1}, the highest record for MOPs.[138] Establishing porous MOPs demands elaborated understanding of both intrinsic (confined cavities) and extrinsic (interstitial voids) pores. Several recent works showed the higher BET surface area obtained from the control of the amorphization in different metal species.[47,138,139] To create highly porous MOPs, a careful selection of chemically stable SBUs such as Zr-based nodes and robust organic linkers is mandatory, controlling intrinsic cavity stability and inter-cage interactions simultaneously. The use of oxophilic cations such as Zr and Cr cations often yields water-stable MOPs with permanent porosity. The discovery of water-stable SBUs with diverse coordination geometry is critical to promote the variety of MOPs.

A unique advantage of MOPs as porous adsorbents is not only the robustness of the desired SBU but also the adjustment of arrangement between the cages for the connection of extrinsic pores. Considering that most of the MOP crystals are held together by weak intermolecular interactions, the control of the packing of MOPs is still challenging to modulate their porous

Table 4 Selected characteristics and functions of MOFs, MOPs, and POCs

Characteristics	MOFs	MOPs	POCs
Porosity	Microporous to mesoporous; up to ~8000 m^2 g^{-1}	Non-porous or microporous; up to ~1300 m^2 g^{-1}	Typically microporous; up to ~3000 m^2 g^{-1}
Applications	Highly applicable to areas such as catalysis, gas separation, bio/energy-related applications, to name a few	Similar, but rather limited applications, compared to MOFs	Particularly, important in molecular separation
Diversity	SBU and linker modulation has been well developed; multivariate MOFs; high structural diversity	Only 14 types of polyhedra; limited choice of SBUs and linkers	Cage type and chemical bonding could be modulated; limited types of cage shapes
Chemical stability	Poor to good; number of water-stable MOFs is rapidly growing	Generally unstable in water; highly stable MOPs are exceptionally rare	Generally unstable; stability could be enhanced by modification of chemical bonding
Processability	Insoluble in solvents	Soluble in specific solvents for some MOPs; applicable to membrane/composites	Soluble in specific solvents; advantageous for membrane applications
Unique properties	Control of structural and chemical properties; isoreticular approach; can be ultraporous	Solution processability; isoreticular approach; can take advantages from the SBU and organic linker	Solution processability; exhibiting polymorphism; possible to co-crystallize
Potential challenges	Commercialization; reproducible and large-scale applications	Establishment of active research area; structural diversity; chemical stability and high permanent porosity	Establishment of active research area; chemical stability

 This journal is © The Royal Society of Chemistry 2021

Published on 09 2020. Downloaded on 10/09/2024 14:36:19.

nature and chemical environment in exterior pores. Yuan *et al.* reported the enhancement of stability and porosity using the control of hydrogen bonding connectivity of Zr-based MOPs.[187] Bloch *et al.* synthesized an ionic salt from the mixing of negatively charged **cuo**-MOP and positively charged Zr-based **tet**-MOP.[188] The novel strategies to regulate interactions such as hydrogen bonding and ionic interactions will expand the number of porous MOP family.

Cage-shaped molecules are attractive because of their prominent properties, especially molecular recognition and encapsulation using the inner cavities. The inner pore in MOPs has great potential for new applications. MOPs can be considered as intermediate porous materials between MOFs and porous organic cages (POCs).[189,190] Solution-processability of POCs and MOPs as the porous membrane was nicely demonstrated in the literature.[118,191,192] From the diversity of SBUs and organic linkers, modular design is the unique strength of MOPs. These new MOPs allow us to explore an essential advantage of MOPs, solution processability, a feature highly desired for industrial applications.

MOFs are well established and widely used in highly active research fields encompassing broad areas of fundamental and materials sciences, while the research areas of MOPs are less explored compared to MOF counterparts. Recently, interesting examples of discrete cages of MOP have been reported for special applications, which are difficult to be accessed by MOFs.[46,101,140,192–196] Further efforts for the discovery of new types of MOP are necessary to enrich the specific applications for MOP chemistry. The characteristics, functions, and potential challenges for MOFs, MOPs, and POCs are compared in Table 4.

The last point is the expansion of topological blueprints for MOPs, similar to coordination cages and MOFs. Only fourteen types of polyhedra were discovered in MOP assembly. This number is significantly lower than that of numerous topologies in over 80 000 MOF crystal structures. Several recent trends in MOPs could be identified in the review. One trend is the use of 5-c metal nodes, enabling us to build a new type of MOP like icosahedron. Inspired by numerous pyridyl-based cage compounds reported by Fujita *et al.*, new linkers with the bent angle slightly higher than 120° could also be tested much more frequently in MOP synthesis. The most popular MOPs, **cuo**-MOPs, have 120° linkers capable of accommodating functional groups at 5-position without hindering the formation of MOPs. If one recalls that 120° is not the ideal angle for constructing a cuboctahedron, the angle variation in the choice of linkers for MOPs could also be interesting, which might narrow the gap between protein assembly and MOP assembly. We strongly believe that there is ample room for MOP chemists to create MOPs with giant cavities through extreme self-assembly.[170–175]

Conflicts of interest

There are no conflicts of interest to declare.

Acknowledgements

This work was supported by the National Research Foundation of Korea (NRF-2016R1A5A1009405 and 2020R1A2C3008226), Korea Environment Industry & Technology Institute (KEITI) through Public Technology Program based on Environmental Policy Program, funded by Korea Ministry of Environment (MOE) (2018000210002). We would like to thank Si Hyun Kim for his help with the visualization of polyhedra.

References

1 S. Alvarez, *Dalton Trans.*, 2005, 2209–2233.
2 B. Artmann, *Math. Intell.*, 1993, **15**, 52–53.
3 National Research Institute of Cultural Heritage, *Sul, Korean Alcoholic Beverages*, 2013, pp. 9–10.
4 F. M. D. Cornford, *Plato's Cosmology: The Timaeus of Plato*, Routledge, 2014.
5 P. Barker and B. R. Goldstein, *Osiris*, 2001, **16**, 88–113.
6 J.-P. Luminet, J. R. Weeks, A. Riazuelo, R. Lehoucq and J.-P. Uzan, *Nature*, 2003, **425**, 593–595.
7 H. W. Kroto, J. R. Heat, S. C. O'Brien, R. F. Curl and R. E. Smally, *Nature*, 1985, **318**, 162–163.
8 D. L. D. Casper and A. Klug, *Cold Spring Harbor Symp. Quant. Biol.*, 1962, **27**, 1–24.
9 D. Shechtman, I. Blech, D. Gratias and J. W. Cahn, *Phys. Rev. Lett.*, 1984, **53**, 1951–1953.
10 Y. Sun and Y. Xia, *Science*, 2002, **298**, 2176–2179.
11 M. Eddaoudi, J. Kim, J. B. Wachter, H. K. Chae, M. O'Keeffe and O. M. Yaghi, *J. Am. Chem. Soc.*, 2001, **123**, 4368–4369.
12 M. J. Kalmutzki, N. Hanikel and O. M. Yaghi, *Sci. Adv.*, 2018, **4**, eaat9180.
13 J. Jiao, C. Tan, Z. Li, Y. Liu, X. Han and Y. Cui, *J. Am. Chem. Soc.*, 2018, **140**, 2251–2259.
14 C. Tan, J. Jiao, Z. Li, Y. Liu, X. Han and Y. Cui, *Angew. Chem., Int. Ed.*, 2018, **57**, 2085–2090.
15 A. C. Sudik, A. R. Millward, N. W. Ockwig, A. P. Côté, J. Kim and O. M. Yaghi, *J. Am. Chem. Soc.*, 2005, **127**, 7110–7118.
16 S. Furukawa, N. Horike, M. Kondo, Y. Hijikata, A. Carné-Sánchez, P. Larpent, N. Louvain, S. Diring, H. Sato, R. Matsuda, R. Kawano and S. Kitagawa, *Inorg. Chem.*, 2016, **55**, 10843–10846.
17 M. Jung, H. Kim, K. Baek and K. Kim, *Angew. Chem., Int. Ed.*, 2008, **47**, 5755–5757.
18 A. Mallick, B. Garai, D. D. Díaz and R. Banerjee, *Angew. Chem., Int. Ed.*, 2013, **52**, 13755–13759.
19 Y. Li, D. Zhang, F. Gai, X. Zhu, Y. Guo, T. Ma, Y. Liu and Q. Huo, *Chem. Commun.*, 2012, **48**, 7946–7948.
20 C. Zhao, N. Wang, L. Wang, H. Huang, R. Zhang, F. Yang, Y. Xie, S. Ji and J.-R. Li, *Chem. Commun.*, 2014, **50**, 13921–13923.
21 Y. N. Yun, M. Sohail, J.-H. Moon, T. W. Kim, K. M. Park, D. H. Chun, Y. C. Park, C.-H. Cho and H. Kim, *Chem. – Asian J.*, 2018, **13**, 631–635.
22 D. J. Tranchemontagne, Z. Ni, M. O'Keeffe and O. M. Yaghi, *Angew. Chem., Int. Ed.*, 2008, **47**, 5136–5147.

Published on 09 2020. Downloaded on 10/09/2024 14:36:19.

23 N. Hosono and S. Kitagawa, *Acc. Chem. Res.*, 2018, **51**, 2437–2446.
24 J. J. Perry IV, J. A. Perman and M. J. Zaworotko, *Chem. Soc. Rev.*, 2009, **38**, 1400–1417.
25 V. Guillerm, D. Kim, J. F. Eubank, R. Luebke, X. Liu, K. Adil, M. S. Lah and M. Eddaoudi, *Chem. Soc. Rev.*, 2014, **43**, 6141–6172.
26 D. Kim, X. Liu and M. S. Lah, *Inorg. Chem. Front.*, 2015, **2**, 336–360.
27 M. Fujita, M. Tominaga, A. Hori and B. Therrien, *Acc. Chem. Res.*, 2005, **38**, 371–380.
28 K. Harris, D. Fujita and M. Fujita, *Chem. Commun.*, 2013, **49**, 6703–6712.
29 M. Yoshizawa, J. K. Klosterman and M. Fujita, *Angew. Chem., Int. Ed.*, 2009, **48**, 3418–3438.
30 S. R. Seidel and P. J. Stang, *Acc. Chem. Res.*, 2002, **35**, 972–983.
31 R. Chakrabarty, P. S. Mukherjee and P. J. Stang, *Chem. Rev.*, 2011, **111**, 6810–6918.
32 D. L. Caulder and K. N. Raymond, *Acc. Chem. Res.*, 1999, **32**, 975–982.
33 N. Ahmad, A. H. Chughtai, H. A. Younus and F. Verpoort, *Coord. Chem. Rev.*, 2014, **280**, 1–27.
34 N. Ahmad, H. A. Younus, A. H. Chunghtai and F. Verpoort, *Chem. Soc. Rev.*, 2015, **44**, 9–25.
35 H. Vardhan, M. Yusubov and F. Verpoort, *Coord. Chem. Rev.*, 2016, **306**, 171–194.
36 M. O'Keeffe, M. A. Peskov, S. T. Ramsden and O. M. Yaghi, *Acc. Chem. Res.*, 2008, **41**, 1782–1789.
37 Informally, the dual of a polyhedron is the polyhedron obtained by inserting new vertices in the old faces and joining them by new edges to vertices in contiguous faces[22] (MOP review by Yaghi and O'Keeffe).
38 C. Bonneau, M. O'Keeffe, D. M. Proserpio, V. A. Blatov, S. R. Batten, S. A. Bourne, M. S. Lah, J. Eon, S. T. Hyde, S. B. Wiggin and L. Öhrström, *Cryst. Growth Des.*, 2018, **18**, 3411–3418.
39 C. Serre, F. Millange, S. Surblé and G. Férey, *Angew. Chem., Int. Ed.*, 2004, **43**, 6286–6289.
40 G. Férey, C. Serre, C. Mellot-Draznieks, F. Millange, S. Surblé, J. Dutour and I. Margiolaki, *Angew. Chem., Int. Ed.*, 2004, **43**, 6296–6301.
41 G. Férey, C. Mellot-Draznieks, C. Serre, F. Millange, J. Dutour, S. Surblé and I. Margiolaki, *Science*, 2005, **309**, 2040–2042.
42 O. M. Yaghi, M. O'Keeffe, N. W. Ockwig, H. K. Chae, M. Eddaoudi and J. Kim, *Nature*, 2003, **423**, 705–714.
43 J. H. Cavka, S. Jakobsen, U. Olsbye, N. Guillou, C. Lamberti, S. Bordiga and K. P. Lillerud, *J. Am. Chem. Soc.*, 2008, **130**, 13850–13851.
44 G. Liu, Z. Ju, D. Yuan and M. Hong, *Inorg. Chem.*, 2013, **52**, 13815–13817.
45 G. Liu, M. Zeller, K. Su, J. Pang, Z. Ju, D. Yuan and M. Hong, *Chem. – Eur. J.*, 2016, **22**, 17345–17350.
46 D. Nam, J. Huh, J. Lee, J. H. Kwak, H. Y. Jeong, K. Choi and W. Choe, *Chem. Sci.*, 2017, **8**, 7765–7771.
47 Z. Ju, G. Liu, Y. S. Chen, D. Yuan and B. Chen, *Chem. – Eur. J.*, 2017, **23**, 4774–4777.
48 G. Liu, Y. Di Yuan, J. Wang, Y. Cheng, S. B. Peh, Y. Wang, Y. Qian, J. Dong, D. Yuan and D. Zhao, *J. Am. Chem. Soc.*, 2018, **140**, 6231–6234.
49 S. Lee, J. H. Lee, J. C. Kim, S. Lee, S. K. Kwak and W. Choe, *ACS Appl. Mater. Interfaces*, 2018, **10**, 8685–8691.
50 W.-H. Xing, H.-Y. Li, X.-Y. Dong and S.-Q. Zang, *J. Mater. Chem. A*, 2018, **6**, 7724–7730.
51 M. T. Pope and A. Müller, *Angew. Chem., Int. Ed. Engl.*, 1991, **30**, 34–48.
52 E. Coronado and C. J. Gómez-García, *Chem. Rev.*, 1998, **98**, 273–296.
53 D.-L. Long, E. Burkholder and L. Cronin, *Chem. Soc. Rev.*, 2007, **36**, 105–121.
54 A. Dolbecq, E. Dumas, C. R. Mayer and P. Mialane, *Chem. Rev.*, 2010, **110**, 6009–6048.
55 D. Du, J. Qin, S. Li, Z. Su and Y. Lan, *Chem. Soc. Rev.*, 2014, **43**, 4615–4632.
56 A. W. Augustynaiak, M. Fandzloch, M. Domingo, I. Łakomska and J. A. R. Navarro, *Chem. Commun.*, 2015, **51**, 14724–14727.
57 Y. Zhang, X. Wang, S. Li, Y. Gong, B. Song, K. Shao and Z. Su, *Chem. Commun.*, 2016, **52**, 9632–9635.
58 Y. Zhang, S. Li, X. Wang, Y. Gong, K. Shao and Z. Su, *Dalton Trans.*, 2016, **45**, 14898–14901.
59 Y. Gong, Y. Zhang, C. Qin, C. Sun, X. Wang and Z. Su, *Angew. Chem., Int. Ed.*, 2019, **58**, 780–784.
60 A. K. Gupta, A. Yadav, A. K. Srivastava, K. R. Ramya, H. Paithankar, S. Nandi, J. Chugh and R. Boomishankar, *Inorg. Chem.*, 2015, **54**, 3196–3202.
61 M. J. Byrnes, M. H. Chisholm and N. J. Patmore, *Inorg. Chem.*, 2005, **44**, 9347–9352.
62 Y. Zhang, X. Wang, E. Zhou, X. Wu, B. Song, K. Shao and Z. Su, *Dalton Trans.*, 2016, **45**, 3698–3701.
63 Y. Zhang, X. Wang, S. Li, B. Song, K. Shao and Z. Su, *Inorg. Chem.*, 2016, **55**, 8770–8775.
64 J. Vicens and V. Böhmer, *Calixarenes: A Versatile Class of Macrocyclic Compounds*, Springer, 2012.
65 R. M. McKinlay, G. W. V. Cave and J. L. Atwood, *Proc. Natl. Acad. Sci. U. S. A.*, 2005, **102**, 5944–5948.
66 P. Jing, S. J. Dalgarno and J. L. Atwood, *Coord. Chem. Rev.*, 2010, **254**, 1760–1768.
67 P. P. Cholewa and S. J. Dalgarno, *CrystEngComm*, 2014, **16**, 3655–3666.
68 K. Xiong, F. Jiang, Y. Gai, D. Yuan, L. Chen, M. Wu, K. Su and M. Hong, *Chem. Sci.*, 2012, **3**, 2321–2325.
69 F. Dai, U. Sambasivam, A. J. Hammerstrom and Z. Wang, *J. Am. Chem. Soc.*, 2014, **136**, 7480–7491.
70 H. Tan, S. Du, Y. Bi and W. Liao, *Inorg. Chem.*, 2014, **53**, 7083–7085.
71 M. Köberl, M. Cokoja, W. A. Herrmann and F. E. Kühn, *Dalton Trans.*, 2011, **40**, 6834–6859.
72 J. R. Li and H. C. Zhou, *Nat. Chem.*, 2010, **2**, 893–898.
73 J. R. Li, A. A. Yakovenko, W. Lu, D. J. Timmons, W. Zhuang, D. Yuan and H. C. Zhou, *J. Am. Chem. Soc.*, 2010, **132**, 17599–17610.

 This journal is © The Royal Society of Chemistry 2021

Published on 09 2020. Downloaded on 10/09/2024 14:36:19.

74 M. D. Young, Q. Zhang and H. C. Zhou, *Inorg. Chim. Acta*, 2015, **424**, 216–220.
75 C. A. Rowland, G. R. Lorzing, E. J. Gosselin, B. A. Trump, G. P. A. Yap, C. M. Brown and E. D. Bloch, *J. Am. Chem. Soc.*, 2018, **140**, 11153–11157.
76 E. J. Gosselin, C. A. Rowland, K. P. Balto, G. P. A. Yap and E. D. Bloch, *Inorg. Chem.*, 2018, **57**, 11847–11850.
77 S. Ma, Y. Niu, X. Zhao and Z. Duan, *Inorg. Chem. Commun.*, 2016, **70**, 10–13.
78 Z. Ni, A. Yassar, T. Antoun and O. M. Yaghi, *J. Am. Chem. Soc.*, 2005, **127**, 12752–12753.
79 S. Mollick, S. Mukherjee, D. Kim, Z. Qiao, A. V. Desai, R. Saha, Y. D. More, J. Jiang, M. S. Lah and S. K. Ghosh, *Angew. Chem., Int. Ed.*, 2019, **58**, 1041–1045.
80 S. A. Boer, K. F. White, B. Slater, A. J. Emerson, G. P. Knowles, W. A. Donald, A. W. Thornton, B. P. Ladewig, T. D. M. Bell, M. R. Hill, A. L. Chaffee, B. F. Abrahams and D. R. Turner, *Chem. – Eur. J.*, 2019, **25**, 8489–8493.
81 N. Hosono, K. Omoto and S. Kitagawa, *Chem. Commun.*, 2017, **53**, 8180–8183.
82 S. T. Zhang, J. Zhang, X. X. Li, W. H. Fang and G. Y. Yang, *J. Am. Chem. Soc.*, 2010, **132**, 15102–15103.
83 Y. Bi, S. Wang, M. Liu, S. Du and W. Liao, *Chem. Commun.*, 2013, **49**, 6785–6787.
84 Y. Gong, W. Chen, L. Zhao, K. Shao, X. Wang and Z. Su, *Dalton Trans.*, 2018, **47**, 12979–12983.
85 X. Hang, S. Wang, X. Zhu, H. Han and W. Liao, *CrystEngComm*, 2016, **18**, 4938–4943.
86 Y. Zhang, H. Gan, C. Qin, X. Wang, Z. Su and M. J. Zaworotko, *J. Am. Chem. Soc.*, 2018, **140**, 17365–17368.
87 B. Moulton, J. Lu, A. Mondal and M. J. Zaworotko, *Chem. Commun.*, 2001, 863–864.
88 T. H. Chen, L. Wang, J. V. Trueblood, V. H. Grassian and S. M. Cohen, *J. Am. Chem. Soc.*, 2016, **138**, 9646–9654.
89 J. Yang, M. Lutz, A. Grzech, F. M. Mulder and T. J. Dingemans, *CrystEngComm*, 2014, **16**, 5121–5127.
90 E. Amayuelas, A. Fidalgo-Marijuan, G. Barandika, B. Bazán, M. K. Urtiaga and M. I. Arriortua, *CrystEngComm*, 2015, **17**, 3297–3304.
91 E. Amayuelas, A. Fidalgo-Marijuán, B. Bazán, M. K. Urtiaga, G. Barandika and M. I. Arriortua, *CrystEngComm*, 2016, **18**, 1709–1712.
92 H. Abourahma, A. W. Coleman, B. Moulton, B. Rather, P. Shahgaldian and M. J. Zaworotko, *Chem. Commun.*, 2001, 2380–2381.
93 J. Lee, J. Kwak and W. Choe, *Nat. Commun.*, 2017, **8**, 14070.
94 R. W. Larsen, G. J. McManus, J. J. Perry IV, E. Rivera-Otero and M. J. Zaworotko, *Inorg. Chem.*, 2007, **46**, 5904–5910.
95 H. Kim, M. Oh, D. Kim, J. Park, J. Seong, S. K. Kwak and M. S. Lah, *Chem. Commun.*, 2015, **51**, 3678–3681.
96 G. R. Lorzing, B. A. Trump, C. M. Brown and E. D. Bloch, *Chem. Mater.*, 2017, **29**, 8583–8587.
97 R. Kumar and C. N. R. Rao, *Dalton Trans.*, 2017, **46**, 7998–8003.
98 A. Mallick, B. Garai, D. D. Díaz and R. Banerjee, *Angew. Chem., Int. Ed.*, 2013, **52**, 13755–13759.
99 H. Huang, J.-R. Li, K. Wang, T. Han, M. Tong, L. Li, Y. Xie, Q. Yang, D. Liu and C. Zhong, *Nat. Commun.*, 2015, **6**, 8847.
100 Y.-H. Kang, N. Yan, Z.-Y. Gao, P. Tan, Y. Jiang, X.-Q. Liu and L.-B. Sun, *J. Mater. Chem. A*, 2017, **5**, 5278–5282.
101 Y. H. Kang, X. D. Liu, N. Yan, Y. Jiang, X. Q. Liu, L. B. Sun and J. R. Li, *J. Am. Chem. Soc.*, 2016, **138**, 6099–6102.
102 R. W. Larsen, *J. Am. Chem. Soc.*, 2008, **130**, 11246–11247.
103 C. M. Vetromile, A. Lozano, S. Feola and R. W. Larsen, *Inorg. Chim. Acta*, 2011, **378**, 36–41.
104 K. Mohomed, H. Abourahma, M. J. Zaworotko and J. P. Harmon, *Chem. Commun.*, 2005, 3277–3279.
105 L.-B. Sun, J.-R. Li, W.-G. Lu, Z.-Y. Gu, Z.-P. Luo and H.-C. Zhou, *J. Am. Chem. Soc.*, 2012, **134**, 15923–15928.
106 K. Mohomed, T. G. Gerasimov, H. Abourahma, M. J. Zaworotko and J. P. Harmon, *Mater. Sci. Eng., A*, 2005, **409**, 227–233.
107 Z. Niu, S. Fang, X. Liu, J.-G. Ma, S. Ma and P. Cheng, *J. Am. Chem. Soc.*, 2015, **137**, 14873–14876.
108 C. Zhao, N. Wang, L. Wang, S. Wang, H. Fan, F. Yang, S. Ji, J. R. Li and J. Yu, *AIChE J.*, 2016, **62**, 3706–3716.
109 H. Furukawa, J. Kim, N. W. Ockwig, M. O'Keeffe and O. M. Yaghi, *J. Am. Chem. Soc.*, 2008, **130**, 11650–11661.
110 H.-N. Wang, X. Meng, G.-S. Yang, X.-L. Wang, K. Z. Shao, Z.-M. Su and C.-G. Wang, *Chem. Commun.*, 2011, **47**, 7128–7130.
111 X. Liu, X. Wang, A. V. Bavykina, L. Chu, M. Shan, A. Sabetghadam, H. Miro, F. Kapteijn and J. Gascon, *ACS Appl. Mater. Interfaces*, 2018, **10**, 21381–21389.
112 G. J. McManus, Z. Wang and M. J. Zaworotko, *Cryst. Growth Des.*, 2004, **4**, 11–13.
113 W. Wei, W. Li, X. Wang and J. He, *Cryst. Growth Des.*, 2013, **13**, 3843–3846.
114 J. Ma, Y. Ying, Q. Yang, Y. Ban, H. Huang, X. Guo, Y. Xiao, D. Liu, Y. Li, W. Yang and C. Zhong, *Chem. Commun.*, 2015, **51**, 4249–4251.
115 B. Garai, A. Mallick, A. Das, R. Mukherjee and R. Banerjee, *Chem. – Eur. J.*, 2017, **23**, 7361–7366.
116 C. R. P. Fulong, J. Liu, V. J. Pastore, H. Lin and T. R. Cook, *Dalton Trans.*, 2018, **47**, 7905–7915.
117 Y. Ke, D. J. Collins and H. C. Zhou, *Inorg. Chem.*, 2005, **44**, 4154–4156.
118 M. Kitchin, J. Teo, K. Konstas, C. H. Lau, C. J. Sumby, A. W. Thornton, C. J. Doonan and M. R. Hill, *J. Mater. Chem. A*, 2015, **3**, 15241–15247.
119 O. Barreda, G. Bannwart, G. P. A. Yap and E. D. Bloch, *ACS Appl. Mater. Interfaces*, 2018, **10**, 11420–11424.
120 D. Zhao, S. Tan, D. Yuan, W. Lu, Y. H. Rezenom, H. Jiang, L. Q. Wang and H. C. Zhou, *Adv. Mater.*, 2011, **23**, 90–93.
121 N. Ahmad, H. A. Younus, A. H. Chughtai, K. V. Hecke, M. Danish, Z. Gaoke and F. Verpoort, *Sci. Rep.*, 2017, **7**, 832.
122 M. Tonigold, J. Hitzbleck, S. Bahnmüller, G. Langstein and D. Volkmer, *Dalton Trans.*, 2009, 1363–1371.
123 M. Tonigold and D. Volkmer, *Inorg. Chim. Acta*, 2010, **363**, 4220–4229.
124 H. Furukawa, J. Kim, K. E. Plass and O. M. Yaghi, *J. Am. Chem. Soc.*, 2006, **128**, 8398–8399.

Published on 09 2020. Downloaded on 10/09/2024 14:36:19.

125 E. V. Perez, K. J. Balkus, J. P. Ferraris and I. H. Musselman, *J. Membr. Sci.*, 2014, **463**, 82–93.
126 J. J. Perry IV, V. C. Kravtsov, M. J. Zaworotko and R. W. Larsen, *Cryst. Growth Des.*, 2011, **11**, 3183–3189.
127 M.-S. Kim, J. Perry IV, T. C. M. Julien, E. Marangon, C. Manouat, J. F. Eubank and J. P. Harmon, *J. Mater. Chem. A*, 2015, **3**, 13215–13225.
128 O. Barreda, G. A. Taggart, C. A. Rowland, G. P. A. Yap and E. D. Bloch, *Chem. Mater.*, 2018, **30**, 3975–3978.
129 N. Hosono, M. Gochomori, R. Matsuda, H. Sato and S. Kitagawa, *J. Am. Chem. Soc.*, 2016, **138**, 6525–6531.
130 D. Zhao, D. Q. Yuan, R. Krishna, J. M. van Baten and H. C. Zhou, *Chem. Commun.*, 2010, **46**, 7352–7354.
131 T.-F. Liu, Y.-P. Chen, A. A. Yakovenko and H.-C. Zhou, *J. Am. Chem. Soc.*, 2012, **134**, 17358–17361.
132 K. Omoto, N. Hosono, M. Gochomori and S. Kitagawa, *Chem. Commun.*, 2018, **54**, 7290–7293.
133 J. Park, L. B. Sun, Y. P. Chen, Z. Perry and H. C. Zhou, *Angew. Chem., Int. Ed.*, 2014, **53**, 5842–5846.
134 M. Zhang, W. Lu, J. R. Li, M. Bosch, Y. P. Chen, T. F. Liu, Y. Liu and H. C. Zhou, *Inorg. Chem. Front.*, 2014, **1**, 159–162.
135 J. Bae, K. Baek, D. Yuan, W. Kim, K. Kim, H. C. Zhou and J. Park, *Chem. Commun.*, 2017, **53**, 9250–9253.
136 H. Jung, D. Moon and H. Chun, *Bull. Korean Chem. Soc.*, 2011, **32**, 2489–2492.
137 G. Lal, S. J. Lee, D. M. Spasyuk and G. K. H. Shimizu, *Chem. Commun.*, 2018, **54**, 1722–1725.
138 G. R. Lorzing, E. J. Gosselin, B. A. Trump, A. H. P. York, A. Sturluson, C. A. Rowland, G. P. A. Yap, C. M. Brown, C. M. Simon and E. D. Bloch, *J. Am. Chem. Soc.*, 2019, **141**, 12128–12138.
139 J. Park, Z. Perry, Y. P. Chen, J. Bae and H. C. Zhou, *ACS Appl. Mater. Interfaces*, 2017, **9**, 28064–28068.
140 A. Carné-Sánchez, G. A. Craig, P. Larpent, T. Hirose, M. Higuchi, S. Kitagawa, K. Matsuda, K. Urayama and S. Furukawa, *Nat. Commun.*, 2018, **9**, 2506.
141 R. Kawano, N. Horike, Y. Hijikata, M. Kondo, A. Carné-Sánchez, P. Larpent, S. Ikemura, T. Osaki, K. Kamiya, S. Kitagawa, S. Takeuchi and S. Furukawa, *Chem*, 2017, **2**, 393–403.
142 A. Carné-Sánchez, J. Albalad, T. Grancha, I. Imaz, J. Juanhuix, P. Larpent, S. Furukawa and D. Maspoch, *J. Am. Chem. Soc.*, 2019, **141**, 4094–4102.
143 J. Albalad, A. Carné-Sánchez, T. Grancha, L. Hernández-López and D. Maspoch, *Chem. Commun.*, 2019, **55**, 12785–12788.
144 J. M. Teo, C. J. Coghlan, J. D. Evans, E. Tsivion, M. Head-Gordon, C. J. Sumby and C. J. Doonan, *Chem. Commun.*, 2016, **52**, 276–279.
145 Z. Zhang, L. Wojtas and M. J. Zaworotko, *Chem. Sci.*, 2014, **5**, 927–931.
146 M. Liu, W. Liao, C. Hu, S. Du and H. Zhang, *Angew. Chem., Int. Ed.*, 2012, **51**, 1585–1588.
147 F.-R. Dai and Z. Wang, *J. Am. Chem. Soc.*, 2012, **134**, 8002–8005.
148 S. Du, C. Hu, J.-C. Xiao, H. Tan and W. Liao, *Chem. Commun.*, 2012, **48**, 9177–9179.
149 S. Du, T.-Q. Yu, W. Liao and C. Hu, *Dalton Trans.*, 2015, **44**, 14394–14402.
150 W. Gong, D. Chu, H. Jiang, X. Chen, Y. Cui and Y. Liu, *Nat. Commun.*, 2019, **10**, 600.
151 M. J. Prakash, Y. Zou, S. Hong, M. Park, M. N. Bui, G. H. Seong and M. S. Lah, *Inorg. Chem.*, 2009, **48**, 1281–1283.
152 M. Paul, N. N. Adarsh and P. Dastidar, *Cryst. Growth Des.*, 2014, **14**, 1331–1337.
153 Z. Chen, X. Liu, A. Wu, Y. Liang, X. Wang and F. Liang, *RSC Adv.*, 2016, **6**, 9911–9915.
154 Y.-C. He, J. Yang, W.-Q. Kan and J.-F. Ma, *CrystEngComm*, 2013, **15**, 848–851.
155 J. Huang, L. Liu, Y. Yang, Y. Li, L. Wang, S. Xiang, Z. Yao and Z. Zhang, *Chem. Commun.*, 2019, **108**, 107540.
156 D. Geng, X. Han, Y. Bi, Y. Qin, Q. Li, L. Huang, K. Zhou, L. Song and Z. Zheng, *Chem. Sci.*, 2018, **9**, 8535–8541.
157 It is difficult to accept that the **trp** MOP is designed from building units since only one type of organic linker was used for the preparation of a polyhedron of transitivity (1,2,2).
158 S. Wang, X. Gao, X. Hang, X. Zhu, H. Han, W. Liao and W. Chen, *J. Am. Chem. Soc.*, 2016, **138**, 16236–16239.
159 J.-R. Li and H.-C. Zhou, *Angew. Chem., Int. Ed.*, 2009, **48**, 8465–8468.
160 O. Delgado-Friendrichs and M. O'Keeffe, *Acta Crystallogr., Sect. A: Found. Adv.*, 2017, **73**, 227–230.
161 N. Xu, H. Gan, C. Qin, X. Wang and Z. Su, *Angew. Chem., Int. Ed.*, 2019, **58**, 4649–4653.
162 X. Hang, B. Liu, X. Zhu, S. Wang, H. Han, W. Liao, Y. Liu and C. Hu, *J. Am. Chem. Soc.*, 2016, **138**, 2969–2972.
163 D. K. Chand, K. Biradha, M. Fujita, S. Sakamoto and K. Yamaguchi, *Chem. Commun.*, 2002, 2486–2487.
164 Z. Lu, C. B. Knobler, H. Furukawa, B. Wang, G. Liu and O. M. Yaghi, *J. Am. Chem. Soc.*, 2009, **131**, 12532–12533.
165 M. Tominaga, K. Suzuki, M. Kawano, T. Kusukawa, T. Ozeki, S. Sakamoto, K. Yamaguchi and M. Fujita, *Angew. Chem., Int. Ed.*, 2004, **43**, 5621–5625.
166 D. Fujita, A. Takahashi, S. Sato and M. Fujita, *J. Am. Chem. Soc.*, 2011, **133**, 13317–13319.
167 K. Harris, D. Fujita and M. Fujita, *Chem. Commun.*, 2013, **49**, 6703–6712.
168 Q. F. Sun, T. Murase, S. Sato and M. Fujita, *Angew. Chem., Int. Ed.*, 2011, **50**, 10318–10321.
169 Q.-F. Sun, J. Iwasa, D. Ogawa, Y. Ishido, S. Sato, T. Ozeki, Y. Sei, K. Yamaguchi and M. Fujita, *Science*, 2010, **328**, 1144–1147.
170 D. Fujita, Y. Ueda, S. Sato, H. Yokoyama, N. Mizuno, T. Kumasaka and M. Fujita, *Chem*, 2016, **1**, 91–101.
171 D. Fujita, Y. Ueda, S. Sato, N. Mizuno, T. Kumasaka and M. Fujita, *Nature*, 2016, **540**, 563–566.
172 P. Li, N. A. Vermeulen, C. D. Malliakas, D. A. Gómez-Gualdrón, A. J. Howarth, B. L. Mehdi, A. Dohnalkova, N. D. Browning, M. O'Keeffe and O. K. Farha, *Science*, 2017, **356**, 624–627.
173 P.-S. Huang, S. E. Boyken and D. Baker, *Nature*, 2016, **537**, 320–327.

 This journal is © The Royal Society of Chemistry 2021

Published on 09 2020. Downloaded on 10/09/2024 14:36:19.

174 Y. Hsia, J. B. Bale, S. Gonen, D. Shi, W. Sheffler, K. K. Fong, U. Nattermann, C. Xu, P.-S. Huang, R. Ravichandran, S. Yi, T. N. Davis, T. Gonen, N. P. King and D. Baker, *Nature*, 2016, **535**, 136–139.
175 J. B. Bale, S. Gonen, Y. Liu, W. Sheffler, D. Ellis, C. Thomas, D. Cascio, T. O. Yeates, T. Gonen, N. P. King and D. Baker, *Science*, 2016, **353**, 389–394.
176 R. M. McKinlay, G. W. V. Cave and J. L. Atwood, *Proc. Natl. Acad. Sci. U. S. A.*, 2005, **102**, 5944–5948.
177 H. Kumari, A. V. Mossine, S. R. Kline, C. L. Dennis, D. A. Fowler, S. J. Teat, C. L. Barnes, C. A. Deakyne and J. L. Atwood, *Angew. Chem., Int. Ed.*, 2012, **51**, 1452–1454.
178 A. S. Rathnayake, K. A. Feaster, J. White, C. L. Barnes, S. J. Teat and J. L. Atwood, *Cryst. Growth Des.*, 2016, **16**, 3562–3564.
179 C. Zhang, R. S. Patil, C. Liu, C. L. Barnes and J. L. Atwood, *J. Am. Chem. Soc.*, 2017, **139**, 2920–2923.
180 C. Zhang, R. S. Patil, T. Li, C. L. Barnes and J. L. Atwood, *Chem. Commun.*, 2017, **53**, 4312–4314.
181 K. Su, M. Wu, D. Yuan and M. Hong, *Nat. Commun.*, 2018, **9**, 4941.
182 S. Pasquale, S. Sattin, E. C. Escudero-Adán, M. Martínez-Belmonte and J. De Mendoza, *Nat. Commun.*, 2012, **3**, 785.
183 F. A. Cotton, L. M. Daniels, C. Lin and C. A. Murillo, *Chem. Commun.*, 1999, 841–842.
184 F. A. Cotton, C. Lin and C. A. Murillo, *Inorg. Chem.*, 2001, **40**, 6413–6417.
185 F. A. Cotton, P. Lei, C. Lin, C. A. Murillo, X. Wang, S.-Y. Yu and Z.-X. Zhang, *J. Am. Chem. Soc.*, 2004, **126**, 1518–1525.
186 G. R. Lorzing, E. J. Gosselin, B. S. Lindner, R. Bhattacharjee, G. P. A. Yap, S. Caratzoulas and E. D. Bloch, *Chem. Commun.*, 2019, **55**, 9527–9530.
187 M. Zhou, G. Liu, Z. Ju, K. Su, S. Du, Y. Tan and D. Yuan, *Cryst. Growth Des.*, 2020, **20**, 4127–4134.
188 E. J. Gosselin, G. E. Decker, A. M. Antonio, G. R. Lorzing, G. P. A. Yap and E. D. Bloch, *J. Am. Chem. Soc.*, 2020, **142**, 9594–9598.
189 T. Tozawa, J. T. A. Jones, S. I. Swamy, S. Jiang, D. J. Adams, S. Shakespeare, R. Clowes, D. Bradshaw, T. Hasell, S. Y. Chong, C. Tang, S. Thompson, J. Parker, A. Trewin, J. Bacsa, A. M. Z. Slawin, A. Steiner and A. I. Cooper, *Nat. Mater.*, 2009, **8**, 973–978.
190 T. Hasell and A. I. Cooper, *Nat. Rev. Mater.*, 2016, **1**, 1–14.
191 Q. Song, S. Jiang, T. Hasell, M. Liu, S. Sun, A. K. Cheetham, E. Sivaniah and A. I. Cooper, *Adv. Mater.*, 2016, **28**, 2629–2637.
192 J. Liu, W. Duan, J. Song, X. Guo, Z. Wang, X. Shi, J. Liang, J. Wang, P. Cheng, Y. Chen, M. J. Zaworotko and Z. Zhang, *J. Am. Chem. Soc.*, 2019, **141**, 12064–12070.
193 J. Lee, D.-W. Lim, S. Dekura, H. Kitagawa and W. Choe, *ACS Appl. Mater. Interfaces*, 2019, **11**, 12639–12646.
194 Y. Fang, J. Li, T. Togo, F. Jin, Z. Xiao, L. Liu, H. Drake, X. Lian and H.-C. Zhou, *Chem*, 2018, **4**, 555–563.
195 T. Grancha, A. Carné-Sánchez, L. Hernández-López, J. Albalad, I. Imaz, J. Juanhuix and D. Maspoch, *J. Am. Chem. Soc.*, 2019, **141**, 18349–18355.
196 S. Mollick, S. Fajal, S. Saurabh, D. Mahato and S. K. Ghosh, *ACS Cent. Sci.*, 2020, **6**, 1534–1541.